Syntenin and CD63 Promote Exosome Biogenesis from the Plasma Membrane by Blocking Cargo Endocytosis

Yiwei Ai[1], Chenxu Guo[1], Marta Garcia-Contreras[1], Laura S. Sánchez B.[1], Andras Saftics[2], Oluwapelumi Shodubi[1], Shankar Raghunandan[1], Junhao Xu[1], Shang Jui Tsai[1], Yi Dong[3], Rong Li[3,4], Tijana Jovanovic-Talisman[2], and Stephen J. Gould[1]*

[1]Department of Biological Chemistry
Johns Hopkins University School of Medicine
Baltimore, MD 21205, USA

[2]Department of Cancer Biology and Molecular Medicine
Beckman Research Institute, City of Hope
Duarte, CA 91010, USA

[3]Department of Cell Biology
Johns Hopkins University School of Medicine,
Baltimore, MD 21205, USA

[4]Mechanobiology Institute and Department of Biological Sciences
National University of Singapore
Singapore 117558, Singapore

Abstract

Exosomes are small extracellular vesicles important in health and disease. Syntenin is thought to drive the endosomal biogenesis of CD63 exosomes by recruiting Alix and the ESCRT machinery to endosome-localized CD63. We find instead that syntenin blocks CD63 endocytosis, allowing CD63 to accumulate at the plasma membrane, thereby increasing its direct budding from the plasma membrane. Consistent with this model, we show that specific and general inhibitors of endocytosis induce the exosomal secretion of CD63 and that endocytosis signals inhibit the vesicular secretion of exosome cargo proteins. Furthermore, we show that CD63 is itself a competitive inhibitor of AP-2-mediated endocytosis, driving the plasma membrane accumulation and exosomal secretion of itself and other lysosome membrane proteins. Our results support the hypothesis that highly-enriched exosome cargo proteins bud primarily from the plasma membrane, that endocytosis inhibits their loading into exosomes, and that syntenin and CD63 regulate the loading of lysosomal proteins into exosomes by an Alix-independent modulation of endocytosis.

Introduction

Exosomes are ~30-150 nm in diameter, have the same topology as the cell, and are highly enriched in specific exosomal proteins, especially the exosomal tetraspanins (e.g. CD81, CD9, and CD63 (*1-3*)) and their associated scaffolds (e.g. syntenin(*2, 4*)). Exosomes are released by all eukaryotic cells, and animals use exosomes for a wide variety of biological processes, including the transmission of signals and molecules to neighboring cells, modification of biofluids and extracellular structures, and protein quality control within exosome-producing cells(*5*). A clear understanding of exosome biogenesis is therefore critical to our understanding of basic cell biology, human health and disease, and the emerging field of exosome-based therapeutics(*6-9*). Human cells also release other types of extracellular vesicles (EVs), both small and large, yet exosomes are unique in their selective enrichment of specific cargo proteins, especially the exosomal tetraspanins.

Of the highly-enriched cargoes found in exosomes, CD63 is thought to be the cargo protein that best defines the exosome biogenesis pathway(*10-13*). It is widely presumed that this pathway requires the endocytosis of CD63 and its accumulation at the endosome membrane, followed by its binding to syntenin, the recruitment of Alix to form a CD63-syntenin-Alix complex, which in turn recruits the *endosomal sorting complexes required for transport* (ESCRT) to the cytoplasmic face of the endosome membrane, presumably to drive the formation of intralumenal vesicles (ILVs) that can later be released as exosomes(*11, 14-22*). Consistent with this model, syntenin binds directly to both CD63 and Alix, with syntenin binding CD63's C-terminal peptide via its C-terminal PDZ domains and C-terminal domain (amino acids 100-293 of syntenin) and binding Alix via its 100 amino acid-long N-terminal domain, which contains three Alix-binding YPLxL motifs(*23*).

Although these binding events provide critical information into the formation of the endosome-localized CD63-syntenin-Alix complex, its currently unclear whether these interactions participate in lysosomal trafficking or exosome biogenesis. After all, CD63 is a key mediator of the lysosomal destruction of many proteins(*24-28*), the CD63-syntenin-Alix complex is essential for the lysosomal delivery of human papillomaviruses(*29*), knockout of syntenin had no on the biogenesis of exosome-sized EVs(*12*), and knockout of Alix had no effect on the biogenesis of exosome-sized EVs(*3*). Furthermore, we have found that the most highly enriched exosome cargoes are all localized to the plasma membrane(*3, 30-33*), that plasma membrane anchors are sufficient to induce the vesicular secretion of exosome cargoes(*30, 32*), that endosome membrane anchors are not(*32*), that redirecting CD63 to the plasma membrane induces its exosomal secretion from the cell(*3, 33*), and that endosome-localized cargoes bud only poorly from cells(*3, 32, 33*). These and other lines of evidence indicate that exosome biogenesis is likely to be mediated by a shared, stochastic mechanism that operates along the spectrum of plasma and endosome membranes, with most exosomes arising by direct budding from the cell surface, and is not an endosome-dependent process(*3, 5, 33*).

Recent studies have shown that knockout of the syntenin gene (SDCBP, for **s**yn**dec**an **b**inding **p**rotein) in human cells or mice results in an ~50% reduction in the exosomal secretion of CD63(*12*). Intriguingly, SDCBP$^{-/-}$ cells are not defective in exosome biogenesis *per se*, as they release the same number of small EVs as control cells, and also show no defect in the exosomal secretion of CD81 or CD9(*12*), which are even more highly enriched in exosomes than CD63 (15-fold and 5-fold, respectively(*3, 33*)). As part of our effort to better understand the molecular mechanisms of exosome biogenesis, we elucidated the molecular mechanism by which syntenin affects the biogenesis of CD63 exosomes. In brief, syntenin drives the biogenesis of CD63 exosomes indirectly rather than directly, and does so by blocking the endocytosis of CD63 from the plasma membrane. Furthermore, we show that endocytosis is a potent inhibitor of the exosomal

secretion of exosome cargo proteins. We also find that level expression of CD63 is itself a potent inhibitor of AP-2-mediated endocytosis that drives the plasma membrane accumulation and exosomal secretion of CD63 and other lysosome membrane proteins. These results have significant implications for the molecular mechanisms of exosome biogenesis, the pleiotropic effects of CD63 expression, and the interpretation of model systems based on high-level CD63 expression.

Results

Syntenin expression induces the exosomal secretion of CD63

Knockout or silencing of the syntenin gene causes a selective defect in the exosomal secretion of CD63(*12, 20*). To determine whether 293F cells were a reasonable model for syntenin's impact on the exosomal secretion of CD63, we knocked out the syntenin gene in 293F cells (***fig. S1***). The resulting 293F/SDCBP$^{-/-}$ cell line displayed the same oddly selective phenotype as other syntenin knockout cells, reducing the exosomal secretion of CD63 but showing no effect on the exosomal secretion of CD9 or CD81 (***fig. S1***).

To better understand why loss of syntenin impairs the exosomal secretion of CD63 but not CD81 or CD9, we next asked whether syntenin was sufficient to induce the exosomal secretion of CD63. Towards this end, we created Tet-on 293F (FtetZ) cell lines that carry doxycycline-inducible, TRE3G-driven transgenes encoding (***i***) syntenin; (***ii***) the syntenin mutant ΔN100syntenin, which lacks the N-terminal 100 amino acids, still binds CD63, but lacks syntenin's Alix-binding sites; or (***iii***) the syntenin mutant syntenin∆C23, which lacks the C-terminal 23 amino acids, retains the ability to bind Alix but no longer binds CD63(*23*). These and control (FtetZ) cells were grown in the absence or presence of doxycycline, followed by collection of cells and exosomes, measurement of transgene-encoded syntenin expression by qRT-PCR (***fig. S2***), and interrogation of cell and exosome samples by immunoblot to measure the exosomal secretion of CD63, CD81, and CD9 (***Fig. 1A-C***).

In the absence of doxycycline, all three syntenin transgene-encoded mRNAs were expressed at similar levels (***fig. S2***). This baseline level of syntenin transgene expression was quite low, as FtetZ::syntenin cells had the same amount of syntenin as FtetZ control cells (***Fig. 1A***). Nevertheless, the low baseline expression of ΔN100syntenin triggered a significant increase in the exosomal secretion of CD63, indicating that this mutant form of syntenin was a particularly potent inducer of CD63 exosome biogenesis. Furthermore, when these same cells were grown in the presence of doxycycline, we found that syntenin and ΔN100syntenin both had this effect (***Fig. 1B***). The syntenin-induced exosomal secretion of CD63 was also selective to CD63, as high-level expression of syntenin or ΔN100syntenin had no effect on the exosomal secretion of either CD81 or CD9 (***Fig. 1A-C***). This effect was eliminated by deleting the C-terminal 23 amino acids of syntenin, a mutation that lacks CD63-binding activity(*23*), as high-level expression of syntenin∆C23 was unable to induce the exosomal secretion of CD63.

It should be noted that CD81 and CD9 are loaded into exosomes far more efficiently than CD63, ~15-fold more in the case of CD81 and ~5-fold more in the case of CD9(*1, 3, 33*). The data presented here reinforce this observation, as the baseline exosomal secretion of CD63 is far less efficient than either CD81 or CD9 (***Fig. 1A, B***). From this perspective, the syntenin-induced exosomal secretion of CD63 raises the possibility that syntenin acts primarily to relieve a repressor of CD63's exosomal secretion, allowing CD63 to finally bud from cells at an efficiency comparable to that of its cousin tetraspanins CD81 and CD9. Similar results were also observed in mouse

NIH3T3 fibroblasts (***fig. S3***), providing yet more evidence that syntenin-mediated biogenesis of CD63 exosomes is a conserved aspect of exosome biogenesis.

Syntenin induces the exosomal secretion of CD63 by blocking its endocytosis

We previously discovered that redirecting CD63 to the plasma membrane induced the exosomal secretion of CD63 by ~6-fold(*3, 33*), an increase similar to what we observed above in response to syntenin expression in 293F and NIH3T3 cells. These similarities raised the possibility that syntenin was driving the exosomal secretion of CD63 by increasing its plasma membrane abundance. To explore this possibility, we used flow cytometry to measure the cell surface expression of CD63. In uninduced cells, the low, baseline expression of syntenin had no effect on the cell surface expression of CD63, though baseline expression of ΔN100syntenin increased its cell surface abundance by ~80% (n = 3, p <0.0005) (***Fig. 1D***). This effect was specific for CD63, as these cell lines had nearly identical levels of cell surface CD81 and CD9 (***Fig. 1E, F***). When we examined the doxycycline-induced cells, we found that high-level expression of either syntenin or ΔN100syntenin increased the plasma membrane abundance of CD63 by 3-fold and 5-fold, respectively (n = 3, p <0.0005) whereas synteninΔC23 did not (***Fig. 1G***). The syntenin-mediated induction of surface CD63 was again selective, as the plasma membrane levels of CD81 and CD9 were altered only slightly (***Fig. 1H, I***) (the slight reductions in cell surface staining for CD81 or CD9 correlate with slight declines in their overall abundance in the cell (***Fig. 1B***)).

This increase in the plasma membrane abundance of CD63 was not due to an overall increase in CD63 abundance, as our immunoblot analysis of cell lysates showed that the cell-associated abundance of CD63 did not rise in response to syntenin expression in either 293F cells (***Fig. 1A-C***) or NIH3T3 cells (***fig. S3***). This suggests that syntenin was inducing the plasma membrane accumulation of CD63 by blocking its endocytosis, an activity of syntenin described previously by Latysheva et al.(*23*). These authors demonstrated that syntenin binds directly to the same C-terminal four amino acids of CD63 that comprise its endocytosis signal, -YEVMcooh, a YxxΦ motif peptide that is otherwise bound by the mu2 subunit of the clathrin adaptor AP-2(*23, 34, 35*). To determine whether this mechanism explains the syntenin-induced accumulation of cell surface CD63, we assessed the endocytosis of CD63 in control and syntenin-expressing cell lines. Specifically, these cell lines were seeded onto glass coverslips, incubated in doxycycline-containing media overnight, then shifted to 4ºC, stained with fluorescently tagged antibodies to (green) CD63 and (pink) CD9 (also at 4ºC), washed (also at 4ºC), then either fixed immediately (t = 0) or following incubation at 37ºC for 30 minutes (t = 30). Examination of these cells by confocal fluorescence microscopy confirmed that the control FtetZ cells endocytosed CD63 from the cell surface, leading to the rapid accumulation of CD63 proteins in internal compartments scattered throughout the cytoplasm, while CD9, which lacks an endocytosis signal, remained at the cell surface (***Fig. 1J, N***). In contrast, cells expressing either WT syntenin (***Fig. 1K, O***) or ΔN100syntenin (***Fig. 1L, P***) failed to endocytose CD63, demonstrating that syntenin expression was blocking the endocytosis of CD63. This phenotype was specific for CD63-binding forms of syntenin, as high-level expression of syntenin ΔC23 failed to inhibit the endocytosis of CD63 (***Fig. 1M, Q***).

Syntenin-induced exosome biogenesis is an Alix-independent process

The observation that syntenin drives the exosomal secretion of CD63 by blocking its endocytosis, together with the fact that ΔN100syntenin does so as well, even though it lacks the ability to bind Alix, indicates that Alix is not required for the biogenesis of CD63 exosomes. Given the widespread presumption that a CD63-syntenin-Alix axis plays an essential role in exosome biogenesis, this is a somewhat surprising result. However, we reported recently that Alix knockout cells show little if any defect in exosome biogenesis(*3*). To determine whether syntenin-mediated biogenesis of CD63

exosomes was in fact an Alix-independent phenomenon, we created HtetZ/Alix$^{-/-}$ cells, a Tet-On derivative of Alix$^{-/-}$ HEK293 cells(*3*), then modified the HtetZ/Alix$^{-/-}$ cell line to carry the doxycycline-regulated transgenes encoding syntenin, ΔN100syntenin, or syntenin∆C23. We then examined the sorting and exosomal secretion of CD63 by uninduced and doxycycline-induced cultures of these four cell lines. Flow cytometry established that the absence of Alix had no substantive effect on the syntenin-induced, selective accumulation of plasma membrane CD63, as it was increased by baseline expression of ΔN100syntenin and doxycycline-induced expression of syntenin or ΔN100syntenin, with no substantive effect on cell surface CD81 or CD9 (***fig. S4A-C***). Moreover, when we collected cell and exosome fractions from these cell lines, we found that high level expression of syntenin and ΔN100syntenin still induced the exosomal secretion of CD63 (***fig. S4D, E***). Thus, Alix is not required for the syntenin-induced biogenesis of CD63 exosomes, just as it is not required for biogenesis of exosomes in general, or the exosomal secretion of CD63, CD81, or CD9(*3*).

Syntenin drives the loading of CD63 into plasma membrane-derived, CD81/CD9 exosomes

These observations raise the question of whether high-level expression of syntenin leads to an overall increase in the production of exosomes, or whether it instead increases the loading of CD63 into plasma membrane-derived exosomes. To address the first possibility, we first counted the numbers of exosomes released by syntenin-expressing cells. Towards this end, we grew these same cell lines in chemically-defined media, in the absence or presence of doxycycline, followed by the collection of exosomes and other sEVs by a combination of clarifying filtration, concentrating filtration, and size exclusion chromatography. Exosome yields were then determined by nanoparticle tracking analysis (NTA), which revealed that exosome yields were similar among all four cell lines, regardless of whether they were grown in medium lacking or containing doxycycline (***Fig. 2A***).

To determine whether the increased exosomal secretion of CD63 instead reflected an increase in its exosomal loading into CD81-positive and/or CD9-positive exosomes, most of which bud directly from the plasma membrane(*3, 10, 33*), we interrogated the immunophenotypes of hundreds of individual exosomes collected from doxycycline-induced cells. Single-particle interferometric reflectance (SPIR) imaging provides label-free measurement of individual exosome sizes, and when combined with conventional immunofluorescence microscopy (IFM), allows one to measure the relative abundance of specific proteins in individual exosomes(*3, 33, 36*). We therefore performed SPIR-IFM imaging of CD63 levels on CD81-positive exosomes released by control cells and cells expressing syntenin, ΔN100syntenin, or syntenin∆C23. Specifically, SPIR imaging chips that had been functionalized with antibodies specific for CD81 were used to immunopurify CD81-positive exosomes from the sEV preparations described above. These were then incubated with an Alexa Fluor 647 (AF647)-labeled antibody specific for CD63, washed, fixed, and examined. The resulting SPIR-IFM data is displayed here as a scatter plot of individual vesicle CD63 fluorescence intensity vs exosome size, using a threshold fluorescence intensity to eliminate ambiguous CD63 signals (***Fig. 2B-E***). CD63 was present at high levels on 7% of CD81 exosomes produced by FtetZ::syntenin∆C23 cells (152/2044), on 40% of CD81 exosomes produced by FtetZ::syntenin cells (988/2389), on 35% of CD81 exosomes produced by FtetZ::ΔN100syntenin cells (991/2791), and on 15% of CD81 exosomes produced FtetZ cells (250/1690).

We also performed parallel studies in which CD9-positive exosomes were immunopurified on anti-CD9 antibody-functionalized SPIR imaging chips, stained with AF647-labeled anti-CD63 antibodies, washed, and fixed. When these exosomes were examined by SPIR-IFM imaging, high levels of CD63 were detected on ~6% of CD9 exosomes produced by FtetZ::syntenin∆C23 cells (85/1440), 35% of CD9 exosomes produced by FtetZ::syntenin cells (721/2059), 35% of CD9

exosomes produced by FtetZ::ΔN100syntenin cells (433/1267), and 16% of CD9 exosomes produced by FtetZ cells (159/966) (***Fig. 2F-I***). In short, elevated expression of syntenin or ΔN100syntenin resulted in an increased loading of CD63 into CD81 and CD9 exosomes that can be seen in the proportion of CD81-positive and CD9-positive exosomes that carried significant levels of CD63.

We also examined CD81/CD9-positive exosomes produced by FtetZ and FtetZ::syntenin cells by quantitative single-molecule localization microscopy (qSMLM). Exosomes were once again immunopurified, this time on glass coverslips functionalized with a mixture of anti-CD81 and anti-CD9 antibodies, then stained with a mixture containing an AF647-labeled antibody specific for CD63 and a pair of AF568-labeled antibodies specific for CD81 and CD9. These immunopurified, antibody-stained exosomes were then washed, fixed, and examined by qSMLM. CD81/CD9-positive exosomes produced by doxycycline-induced FtetZ::syntenin cells contained a mean of 18 detected CD63 molecules (coefficient of variation (c.v.) 102%) whereas exosomes produced by doxycycline-induced FtetZ cells contained a mean of 10 detected CD63 molecules (c.v. 102%) (***Fig. 2J***). Not surprisingly, when we calculated the percentage of CD81/CD9-positive exosomes that lacked detectable levels of CD63, we found that it fell from ~35% for exosomes produced by FtetZ cells to ~15% for exosomes produced by syntenin-expressing cells (***Fig. 2K***). As for the deduced size of these exosomes, our data indicated that the exosomes produced by FtetZ cells and FtetZ::syntenin cells had mean diameters of 107 (c.v. 26%) and 113 nm (c.v. 30%), respectively .

General inhibitors of endocytosis induce the exosomal secretion of CD63

Taken together, these observations indiate that the molecular mechanism of syntenin-mediated exosome biogenesis is indirect, inducing the exosomal secretion of CD63 by suppressing the inhibitory effect of its endocytosis from the plasma membrane. If this hypothesis is correct, then blocking CD63 endocytosis by other mechanisms should also induce a selective increase in the exosomal secretion of CD63. As noted above, CD63 is constitutively endocytosed by virtue of its YxxΦ-type endocytosis signal (YEVMcooh), which is bound directly by the mu2 subunit of the clathrin adaptor AP-2(*35, 37-39*). We therefore generated a 293F cell line mutated in AP2M1, the gene that encodes AP-2 mu2 subunit, with one allele carryiong a large null deletion mutation whil the second allele carried a 1 codon deletion in a conserved hydrophobic residue of the protein (ΔIle63) (***fig. S5***). This cell was tested for its ability to endocytose CD63 by growing the control 293F cell line and the F/AP2M1$^{-/-}$ cell line on glass coverslips, then chilling them to 4ºC, incubating them with fluorescently tagged antibodies specific for CD63 and CD9 (also at 4ºC), then washing the cells and fixed them either immediately (t = 0) or after a 30 minutes-long incubation at 37ºC (t = 30). Examination of these cells by confocal immunofluorescence microscopy confirmed that 293F cells rapidly endocytosed CD63 from the cell surface (***Fig. 3A, B***) and established that the F/AP2M1$^{-/-}$ cells did not (***Fig. 3C, D***). As expected, this defect in CD63 endocytosis led to an ~4-fold increase in the abundance of CD63 at the plasma membrane, as determined by flow cytometry (***Fig. 3E***). Furthermore, immunoblot analysis of cell and exosome fractions collected from 293F and F/AP2M1$^{-/-}$ cells showed that this inhibition of CD63 endocytosis led to a significant increase in the loading of CD63 into exosomes (***Fig. 3F, G***), providing direct evidence that inhibition of endocytosis is sufficient to induce a selective increase in the exosomal secretion of CD63.

As an independent test this hypothesis, we asked whether a mechanistically distinct inhibitor of endocytosis would also induce the exosomal secretion of CD63. Actin polymerization plays a critical role in protein endocytosis by providing a driving force for membrane invagination(*40-44*). As a result, several modes of protein endocytosis are inhibited by latrunculin A, which sequesters actin monomers and inhibits actin polymerization. We therefore grew 293F cells in media lacking or containing latrunculin A, collected their exosomes, and interrogated these exosome samples by

immunoblot for CD63, CD81, and CD9. Addition of latrunculin had no effect on the exosomal secretion of CD81 but increased the exosomal secretion of CD63 by ~7-fold (***Fig. 3H, I***), showing once again that endocytosis inhibition induces the exosomal secretion of CD63 but not CD81. As for the latrunculin-induced increase in exosomal CD9, this ~30% increase may explain why CD9 shows more endolysosomal staining than CD81 in 293 cells (*3, 33*).

Endocytosis signals inhibit exosome cargo protein budding

The antagonistic effect of endocytosis on the exosomal secretion of CD63 has profound implications for the mechanisms of exosome biogenesis. For example, it predicts that the presence of an endocytosis signal will limit the exosomal secretion of any protein to which it is attached, even an exosome cargo protein that is otherwise efficiently secreted from the cell in exosomes. Some evidence for this can be found in our previous analysis of a CD9 protein carrying the C-terminus of CD63(*3, 32, 33*), but that study did not examine the effect of different types of YxxΦ-type signals, nor did it explore the role of expression on their exosomal secretion. To address these issues, we used Cas9-mediated gene editing to generate a CD9$^{-/-/-}$ 293F cell line (***fig. S6***), converted it to a Tet-on cell line (FtetZ/CD9$^{-/-/-}$), and then created derivatives of this FtetZ/CD9$^{-/-/-}$ cell line that carry doxycycline-regulated transgenes designed to express WT CD9 or mutant forms of CD9. These mutant forms of CD9 included CD9-YQRF, which has high affinity for the mu2 subunit of AP-2(*35*), CD9-YQTI, which also binds the mu2 protein but has higher affinity for the mu3 subunit of AP-3(*35*), CD9-YEVM, which has high yet competing affinities for both AP-2 and syntenin(*23, 35*), and CD9-AEMV, which lacks the essential tyrosine for binding to clathrin adaptors and also lacks the EVM motif required for binding syntenin.

Interrogation of mRNA levels by qRT-PCR demonstrated that all five cell lines expressed a similar amount of transgene-encoded CD9 mRNA in the absence of doxycycline (***fig. S7***). As expected, WT CD9 and CD9-AEMV were efficiently secreted from the cell in exosomes, as expected from the high efficiency with which CD9 normally buds from the cell in exosomes(*2, 3, 33*) (***Fig. 4A***). In contrast, we were unable to detect CD9-YQRF, CD9-YQTI, or CD9-YEVM in either the exosome or cell lysates, indicating that these endocytosed forms of CD9 had been rapidly degraded. This degradation of CD9-YQRF, CD9-YQTI, and CD9-YEVM was largely suppressed by the addition of bafilomycin A, an inhibitor of the vacuolar ATPase (***fig. S8***), indicating CD9 was being degraded by the canonical plasma membrane-to-lysosome degradation pathway(*45, 46*).

In contrast to these results, doxycycline-induced expression of CD9-YQRF, CD9-YQTI, or CD9-YEVM saturated their plasma membrane-to-lysosome degradation, allowing them to accumulate nearly to the level of CD9 and CD9-AEMV within the cell (***Fig. 4B***). This allowed us to now calculate the relative efficiency (cell/exosome ratio) with which each CD9 protein was loaded into exosomes (***Fig. 4C***). This revealed that CD9 and CD9-AEMV were loaded into exosomes at ~3-fold greater efficiency than the YxxΦ motif-containing forms of CD9 ($n = 3$, $p < 0.005$), confirming our previous discovery that the addition of endocytosis signals inhibits the vesicular secretion of exosome cargo proteins(*3, 33*).

Previous studies have established that AP-2-mediated endocytosis is sensitive to competitive saturation, and that high-level expression of an AP-2-binding ligand can inhibit its own endocytosis(*47-49*). To determine whether this might explain the exosomal secretion of YxxΦ motif-containing forms of CD9, we used flow cytometry to measure the plasma membrane abundance of these five CD9 proteins in both uninduced and doxycycline-induced cells. In the absence of doxycycline, CD9 and CD9-AEMV were abundant at the plasma membrane, whereas CD9-YQRF, CD9-YQTI, or CD9-YEVM showed only slightly more CD9 staining than the control CD9$^{-/-/-}$ cell line (***Fig. 4D***). In the presence of doxycycline, CD9 and CD9-AEMV were ~5-fold (n

= 3, $p < 0.0005$) more abundant at the cell surface than CD9-YQRF, CD9-YQTI, or CD9-YEVM (***Fig. 4E, F***). However, the difference in plasma membrane abundance induced by doxycycline was far greater for the CD9-YQRF, CD9-YQTI, and CD9-YEVM proteins was ~100-fold but only ~3-fold for CD9 and CD9-AEMV (***Fig. 4G***), raising the possibility that the low but significant exosomal secretion CD9-YQRF, CD9-YQTI, and CD9-YEVM occurred by direct budding from the plasma membrane rather than the endocytosis/exocytosis route of ILV release (***Fig. 4B***).

CD63 is an expression-dependent regulator of AP-2-mediated endocytosis and exosome content

The preceding observations raise the possibility that CD63, which naturally contains a YxxΦ-type endocytosis signal, might inhibit its own endocytosis. We therefore created FtetZ/CD63$^{-/-}$ cells, a Tet-on derivative of a CD63$^{-/-}$ 293F cell line(*50*), then generated a derivative of FtetZ/CD63$^{-/-}$ cells that carries a doxycycline-regulated CD63 transgene. The resulting FtetZ/CD63$^{-/-}$::CD63 cells were then seeded onto glass coverslips, incubated overnight in normal media or media supplemented with doxycycline, chilled to 4ºC, incubated with fluorescently-labeled antibodies specific for CD63, washed, and then fixed either immediately (t = 0) or after a 30 minutes-long incubation at 37ºC (t = 30). Examination of these cells by confocal fluorescence microscopy revealed that CD63 was rapidly endocytosed by uninduced FtetZ/CD63$^{-/-}$::CD63 cells (***Fig. 5A, B***) whereas doxycycline-induced expression of CD63 inhibited its own endocytosis (***Fig. 5C, D***).

We next tested whether the level of CD63 expression affected the plasma membrane abundance of Lamp1 or Lamp2, two other lysosome associated membrane proteins that carry YxxF-type endocytosis signals, as well as how other YxxF motifs might affect these results. For these experiments we generated three additional FtetZ/CD63$^{-/-}$ cell lines that carry doxycycline-inducible CD63 transgenes with substitutions in its YEVMcooh motif, specifically (***i***) CD63-YQRF, a high-affinity ligand for AP-2 mu2(*35*); (***ii***) CD63-YQTI, a high-affinity ligand for AP-3 mu3(*35*); and (***iii***) CD63-AEMV, which lacks residues important for binding to AP-2, AP-3, and syntenin(*23, 35*). To measure the abundance of these CD63 proteins at the plasma membrane, each cell line was processed for flow cytometry following the staining of the surface of live cells. At baseline, cells expressing CD63-YQRF or CD63-YQTI stained only slightly for CD63, indicating that these forms of CD63 were efficiently endocytosed from the plasma membrane (***Fig. 5E***). Although WT CD63 is also endocytosed, it's cell surface abundance was slightly higher than that of CD63-YQRF or CD63-YQTI, presumably as a result of syntenin-mediated inhibition of CD63 endocytosis(*23*). Not surprisingly, CD63-AEMV, which lacks the tyrosine essential for binding AP-2, was ~10-fold more abundant at the plasma membrane than WT CD63 (***Fig. 5E***). At these low baseline levels of CD63 expression, the cell surface levels of Lamp1, Lamp2, CD81, and CD9 were unaffected (***Fig. 5F-I***).

This was not, however, the case for the doxycycline-induced cell lines, all of which stained far more brightly for CD63 (***Fig. 5J***). Moreover, the magnitude of these increases, which were 20-50 fold for WT CD63, CD63-YQRF and CD63-YQTI, indicated that high-level expression of YxxΦ motif-containing forms of CD63 was likely inhibiting AP-2-mediate endocytosis. In support of this hypothesis, we found that high level expression of CD63, CD63-YQRF or CD63-YQTI induced the cell surface accumulation of Lamp1 and Lamp2, two other YxxΦ motif-containing lysosomal membrane proteins (***Fig. K, L***). High level expression of these CD63 proteins had no effect on the cell surface expression of CD81 but did cause a decline in the detection of CD9 (***Fig. 5M, N***).

To determine whether the plasma membrane abundance of these proteins predicts their exosomal secretion, we collected cells and exosomes from uninduced and doxycycline-induced cell cultures, then processed these samples for immunoblot. In the absence of doxycycline, the exosomal secrtion of CD63 proteins corresponded closely to their plasma membrane abundance, as plasma membrane-localized CD63-AEMV was loaded into exosomes at far greater efficiency than WT, which was

itself loaded into exosomes more efficiently than either CD63-YQRF or CD63-YQTI (***Fig. 5O***). Under these conditions, CD9 was found in all exosome samples, albeit in an oddly inverse relationship to the exosomal secretion of CD63, as if CD63 were inhibiting slightly the exosomal release of CD9. As for Lamp1 and Lamp2, their presence in exosomes was at best minimal.

Interestingly, when we interrogated cell and exosome samples from doxycycline-induced cells, we observed that all four CD63 proteins were present at similar levels in both cell and exosome lysates, consistent with their inhibition of AP-2-mediated endocytosis and their plasma membrane accumulation (***Fig. 5B***). Moreover, we found that high-level expression of WT CD63, CD63-YQRF or CD63-YQTI induced a pronounced increase in the exosomal secretion of both Lamp1 and Lamp2. However, the CD63-mediated increase in the exosomal secretion of Lamp1 and Lamp2 was only partly due to their YxxΦ motif, as high-level expression of CD63-AEMV also induced the exosomal secretion of these lysosomal proteins, indicating that CD63 may influence lysosome protein trafficking by means other than its YEVM motif. In fact, this effect may be particularly pronounced for WT CD63, as its expression also appeared to cause some alterations in the cellular and exosomal pools of CD9 and Hsp90.

Co-regulation of syntenin, CD63, and the plasma membrane biogenesis of CD63 exosomes

The preceding results demonstrate that high-level expression of CD63 is sufficient to saturate AP-2 and induce the plasma membrane accumulation and exosomal secretion of CD63 and other YxxΦ motif-containing lysosome membrane proteins. These results raise the possibility that natural variations in CD63 expression might have similar effects, we reviewed publicly available CD63 mRNA expression data, which revealed that CD63 transcript abundance exceeds the threshold of a highly expressed gene (>1000 normalized transcripts per million (nTPM)) in 20 of the 75 cell types and varies by more than 300-fold, from <10 nTPM in neurons to >3000 nTPM in respiratory epithelia (***Table S1***)(*51*). Not surprisingly, cell lines also vary widely in CD63 expression, as CD63 mRNA abundance was 249 nTPM in 293F cells, was as low as 87 nTPM in Daudi cells, and as high as 2373 nTPM in SK-MEL-5 cells. This variation in CD63 expression could also be seen by immunoblot, as SK-MEL-5 cells express far higher levels of CD63 than 293F cells, which express more CD63 protein than Daudi cells (***Fig. 6A***). Interestingly, these variations in CD63 expression were matched by variations in syntenin expression, which was also highest in SK-MEL-5 cells and lowest in Daudi cells. This result led us to test whether there is any other evidence of coordinate regulation of CD63 and syntenin expression, which we did by interrogating >240,000 RNAseq datasets. This analysis showed that CD63 and syntenin mRNA abundance displays a strong positive correlation across 44 distinct sets of normal and cancer tissues (***Fig. S9***).

Given that high-level expression of either CD63 or syntenin inhibit CD63 endocytosis and increase its plasma membrane accumulation and exosomal secretion, their coordinate high level expression in SK-MEL-5 cells predicts that CD63 should be abundant at their plasma membrane and efficiently loaded into their exosomes. Flow cytometry of surface-labeled SK-MEL-5 cells and 293F cells confirmed the first of these predictions, as SK-MEL-5 cells had 13-fold more CD63 at their plasma membrane than 293F cells, even though both cell lines had similar levels of cell surface CD81 and CD9 (***Fig. 6B***). Furthermore, when we collected cell and exosome fractions from these cell lines and interrogated them by immunoblot, we found that SK-MEL-5 cells loaded CD63 into exosomes at 6-fold greater efficiency than 293F cells (***Fig. 6C, D***), demonstrating that naturally occurring elevations in the expression of CD63 and syntenin drive CD63 to the plasma membrane and induce its direct budding from the cell surface.

Discussion

The results presented here show that syntenin's primary role in the biogenesis of CD63 exosomes is to inhibit CD63 endocytosis by binding to the same site on CD63 as AP-2. This competitive interaction inhibits CD63 endocytosis, thereby allowing CD63 to accumulate at the plasma membrane, giving it a greater chance of being loaded into exosomes that are budding directly from the plasma membrane. Thus, we identify the molecular mechanism of syntenin-induced biogenesis of CD63 exosomes to be indirect, independent of Alix, and largely separated from the packaging of cargoes into nascent budding vesicles or their scission from the cell membrane. This indirect, Alix-independent mechanism is supported by a wide array of additional observations, including the increased exosomal secretion of CD63 in response to endocytosis inhibitors, the reduced exosomal secretion of cargoes that carry endocytosis signals, and the increased plasma membrane accumulation and exosomal secretion of AP-2-binding cargoes by their own high-level expression, or by high-level expression of CD63. These findings highlight the shared, stochastic nature of vesicles budding along the continuum of plasma and endosome membranes, the complexity of interactions between the expression of CD63 and syntenin and the dynamics of protein endocytosis and exosome biogenesis, and the system-perturbing effects of CD63-based models for studying exosome biogenesis.

Reassessment of exosome biogenesis

As noted above, the findings presented here expand the empirical support for the shared, stochastic model of exosome biogenesis as a process that operates along the spectrum of plasma and endosome membranes, and primarily from the plasma membrane(*3, 5, 33*). Although we and others have previously generated significant support for this model(*3, 5, 30-33, 52-56*), the present paper adds even more evidence that the plasma membrane is the primary site of exosome biogenesis (***Fig. 7i***), and that endocytosis (***Fig. 7ii***) inhibits the vesicular secretion of exosome cargo proteins, by removing them from the primary site of exosome biogenesis, the plasma membrane. Moreover, we now show that specific and general inhibitors of cargo protein endocytosis (***Fig. 7iii***) indirectly induce the exosomal secretion of these otherwise endocytosed cargoes by allowing them to (***Fig. 7i'***) accumulate at the plasma membrane, their preferred site of exosomal budding from the cell. It should be noted that the prevailing, endosome-dependent model of exosome biogenesis not only failed to predict these experimental results, but is incapable of explaining them (***Table S2***).

It should be noted that this shared, stochastic model applies to a diversity of cell types, and is not merely peculiar to 293 cell lines. For example, we showed here that syntenin-induced exosomal secretion of CD63 occurs in cell lines as distinct as the human 293F cell line and the mouse NIH3T3 fibroblast cell line. Our model applies also to the melanoma cell line SK-MEL-5, which responds to high level expression of CD63 and syntenin by increasing CD63's plasma membrane abundance and exosomal secretion. It also explains the oddly selective exosome biogenesis abnormality observed in SDCBP$^{-/-}$ derivatives of MCF-7 cells and transgenic mice(*12*), and of 293F cells. Moreover, it explains the superior exosomal secretion of plasma membrane-localized exosome cargoes by HEK293 cells, 293F cells, Jurkat T-cells (*32*), Hela cells (*10*), and mouse NIH 3T3 cells(*3, 33*) cells.

The observation that exosome cargoes bud primarily from the plasma membrane is consistent with the large surface area of the plasma membrane, as well as the fact that every 'outward' budding vesicle event at the plasma membrane generates an exosome (outward = away from the cytoplasm). The same cannot be said of ILV biogenesis, most of which are slated for lysosomal destruction(*45, 46*). Thus, when an endocytosed exosome cargo protein is (***Fig. 7iv***) loaded into a nascent ILV, its likely fate is to be (***Fig. 7v***) later delivered to lysosomes and degraded in lysosomes. We observed

this for endocytosed forms of CD9, all of which were efficiently degraded by a V-ATPase-dependent mechanism. This pathway was easily saturated, which is not surprising when one considers that it involves a large number of distinct, separate biochemical processes, including clathrin/AP-2-mediated endocytosis of the cargo from the plasma membrane, uncoating of the endocytic vesicles that carry the cargo, fusion of these endocytic vesicles with early endosomes, loading of the endosome-localized cargo protein into nascent ILVs, fusion of ILV-containing endosomes with lysosomes, and enzymatic hydrolysis of ILV proteins and lipids.

As a result of this slow an saturable process, there is always a stockpile of ILVs not yet degraded, which means that (***Fig. 7vi***) exocytosis of their endolysosomal carriers will release some ILVs as exosomes. Moreover, there is increasing evidence that this *en bloc* release of ILVs can be triggered, such as in response to plasma membrane wound repair and other inducers of intracellular calcium, a process that requires annexin 6(*57*). Other inducers of ILV release are thought to include lysosome poisons, including bafilomycin A(*58*) and viral de-acidifying proteins(*59*). However, it's unclear whether these exocytotic triggers act solely by releasing pre-formed ILVs and how much results from increased exosome budding from the plasma membrane. After all, an acute induction of exocytosis might lead to ILV release but a chronic induction of exocytosis will generate large amount of plasma membrane that are endosomal in nature and still competent for vesicle budding.

Relevance to exosome engineering

In addition to being the most parsimonious explanation of exosome biogenesis, the shared, stochastic model draws a clear roadmap for recombinant exosome engineering. In brief, this model predicts that loading proteins into exosomes involves only three engineerable steps: expression of the cargo, cargo delivery to the plasma membrane, and cargo loading into nascent budding vesicles. As for the secondary, endocytosis/exocytosis route of exosome biogenesis, our model predicts that its an effectively non-engineerable process, for three simple reasons: *first*, high level expression of CD63 or other such cargoes will block AP-2-mediated endocytosis and result in the vast majority of the cargo protein budding directly from the plasma membrane and not via endosomes; *second*, the inhibition of AP-2 will pervert the exosome biogenesis process by trapping lysosomal proteins at the plasma membrane and driving their aberrant loading into exosomes; and *third*, the CD63-mediated inhibition of AP-2-mediated endocytosis is highly likely to perturb cell physiology in general, as AP2M1 is essential for animal life(*60*).

Implications for CD63-based models of exosome biology

Our results also have important practical implications for the design of experiments and the interpretation of data arising from high-level expression of CD63 proteins. To be blunt, our data shows that all experiments involving high-level expression of CD63 carry the unavoidable flaw of inhibiting AP-2-mediated endocytosis, an inhibition already known to have serious deleterious effects on cell physiology in general and lysosome function in particular(*60*), and which we have shown here to also include the perversion of exosome content that comes from increasing the plasma membrane abundance of lysosomal proteins like Lamp1 and Lamp2. For example, many of the transgenic animal models that have been developed for *in vivo* studies of exosome biology are based on high-level expression of CD63(*61-65*). The expression of CD63 in these models, disconnected from the co-ordinate expression of syntenin, is highly likely to suffer from defects in AP-2-mediated endocytosis, aberrant lysosome function, and a perversion of exosome content due to the CD63-induced loading of lysosomal proteins into plasma membrane-derived exosomes. While our findings provide a mechanistic rationale for avoiding the use of such models, caution in their use is already warranted, as systemic expression of CD63 in rats caused a highly penetrant neonatal lethality, while reducing CD63 expression in this same model by a 1/3 allowed female mice to breed and live as along as 4-6 months, though their lifespan was greatly shorted (Wistar

rats normally survive 2.5-3 years)(*61*). Although we have no direct evidence that these rats died because of CD63-induced inhibition of AP-2-mediated endocytosis, AP-2 is essential for animal life(*60*), and thus, inhibition of AP-2 could be the cause their death. Given that all future CD63-based studies will have to account for this possibility, it seems far better to focus instead on the animal models based on CD81, which shows no sign of endocytosis and is the most highly-enriched exosome cargo protein yet described(*1, 3, 33*).

These concerns extend to cell-based models of exosome biogenesis that rely on high-level expression of CD63 proteins, including studies of exosome content, exosome biogenesis, and signal-induced exosome biogenesis (*10, 66-71*). While the experimental design of these studies may have seemed reasonable at the time, our discovery that high-level expression of CD63 inhibits AP-2-mediated endocytosis means that their data and interpretations may now warrant re-evaluation. For example, Mathieu et al. asserted that CD63, Lamp1, Lamp2, and CD9 all bud together into ILVs later released as exosomes, primarily because high-level expression of CD63 led to their co-localization in exosomes, results that we show here are due instead to CD63-mediated inhibition of endocytosis, inducing the plasma membrane accumulation and exosomal secretion of CD63, Lamp1, Lamp2 and CD9 directly from the plasma membrane. Furthermore, our observation that high-level expression of CD63 proteins cause a dramatic reduction in the cell-associated abundance of Lamp1 and Lamp2, even CD63-AEMV, indicates that CD63 has additional effects on lysosome function that are not currently understood. In short, high-level expression of CD63 appears to cause an unavoidable antagonism of endocytosis and perhaps other aspects of cell physiology, introducing experimental artefacts not easily controlled, yet easily avoided by focusing on the more highly enriched exosome cargoes CD81 and CD9.

Mechanism and logic in exosome nomenclature

The model of exosome biogenesis presented here (***Fig. 7***) is mechanistically sound, supported by a wide array of empirical observations presented here and elsewhere(*3, 5, 30-33, 52, 53, 55, 56*), and consistent with the traditional *experimental* definition of the exosome as a small secreted vesicle of ~30-150 nm that has the same topology as the cell and is enriched in exosome cargo proteins(*5, 53, 72*). In contrast to this simple, rational, and workable definition, others have sought to define exosomes and other EVs by their membrane of origin, restricting the term to only those vesicles that can be proved to arise by ILV release, and using the term ectosome for all vesicles that arise from the plasma membrane, a group that includes a numerous types of EVs in addition to the exosomes that bud from the plasma membrane(*10, 13, 22, 73*). However, several considerations indicate that this 'membrane origin' approach to exosome nomenclature has little if any relevance to the underlying biology of exosomes, the way that experiments are actually performed, or the data that they yield. These considerations include the following:

- First, this paper and our previous studies(*3, 5, 33*) demonstrate that the most highly-enriched exosome cargoes, including CD81, CD9, and CD63, all bud from both plasma and endosome membranes in vesicles that have the same size and topology, in ways that vary from one cell type to another, though primarily from the plasma membrane.
- Second, this means that there is no way to know where any individual exosome arose once it has left the cell, which means that the dichotomous approach to exosomes nomenclature has no relation to experimental practice or empirical investigation.
- Third, we and others have shown that the highly enriched exosome proteins vary by 100-fold or more from one exosome to another, dwarfing the relatively modest bulk differences between exosomes that arise from the plasma membrane (more CD81 and CD9) and those that arose first as ILVs.

- Fourth, by separating plasma membrane-derived exosomes from endosome-derived exosomes, calling them by different names creates a false dichotomy between exosome-sized vesicles that have the same size, topology, and share many/most of the same cargoes.
- Fifth, by lumping plasma membrane-derived exosomes with all other plasma membrane-derived EVs, the dichotomous approach to exosome nomenclature inaccurately conflates exosomes with non-exosomal EVs.
- Sixth, the dichotomous approach to exosome biogenesis presumes a dominant role for the endocytosis/exocytosis route in the biogenesis of exosomes that does not exist (***Table S2***) and bears no relation to the techniques that are used for studying exosomes, none of which can separate plasma membrane-derived exosomes from endosome membrane-derived exosomes.

In light of these considerations, the best path forward is for the EV field to accept that all cells bud exosome cargoes and exosomes along a spectrum of plasma and endosome membranes. This would go a long way towards lifting the heavy burden of observational bias that pervades the field, limits experimental designs, and warps data interpretation. More specifically, it would clear the way for extensive application of cargo-based, mechanistic studies of exosome biogenesis without breaking their continuity with past decades of exosome research.

Materials and Methods

Plasmids

The plasmid pJM1463 is based on a pS series plasmid(*54*) and carries a bicistronic ORF encoding rtTAv16-2a-BleoR downstream of the spleen focus forming virus (SFFV) transcriptional control region. The plasmids pYA128, YA129, and pYA130 are Sleeping Beauty transposons based on pITRSB(*54*) that carry two genes: (***i***) an EFS-PuroR gene and (***ii***) a TRE3G regulated gene designed to express syntenin, ΔN100syntenin, or syntenin∆C23, respectively. The plasmids pCG606, pCG732, pCG733, pCG734, and pCG607 are Sleeping Beauty transposons based on pITRSB that carry two genes: (***i***) an EFS-HygR gene and (**ii**) a TRE3G regulated gene designed to express codon optimized CD9 ORFs that encode WT CD9, CD9-YQRF, CD9-YQTI, CD9-AEMV, and CD9-YEVM, respectively. The plasmids pCG602, pMG9, pCG604, and pMG10 are Sleeping Beauty transposons based on pITRSB that carry two genes: (***i***) an EFS-HygR gene and (**ii**) a TRE3G regulated gene designed to express codon optimized ORFs that encode WT CD63, CD63-YQRF, CD63-YQTI, and CD63-AEMV. All genes were synthesized *in vitro*, cloned into the appropriate, expression vectors, and then sequenced in their entirety to ensure the absence of unwanted mutations.

The plasmid used for knockout of the SDCBP gene, pJM1087, was based on pFF(*3*) and contains three genes. The first of these consists of a CMV promoter driving expression of a single long quadricistronic ORF that encodes (***i***) Cas9-3xNLS, (***ii***) a viral 2a peptide, (***iii***) EGFP, (***iv***) another viral 2a peptide, (***v***) the thymidine kinase (tk) from herpes simplex virus (HSV), (***vi***) another viral 2a peptide, and (***vii***) the puromycin resistance protein PuroR(*54*), with the ORF flanked by a pair of loxP sites. The second of these genes consists of the PolIII-transcribed H1 promoter diving expression of a Cas9 gRNA with the target sequence of 5'-ATAAACCTACTTCCATCGTG-3', which is complementary to a sequence in the second coding exon of the SDCBP gene. The third of these genes consists of the PolIII-transcribed 7sk promoter diving expression of a Cas9 gRNA with the target sequence of 5'-GGTTTCTGGTGCACCACTTC-3', which is complementary to a sequence in the third coding exon of the SDCBP gene.

Plasmids carrying genomic DNA (gDNA) amplification products from mutant cell lines were generated by extracting gDNA from single cell clones, amplifying small fragments of the genome surrounding the targeted site, using Taq polymerase. The resulting PCR fragments were checked for proper size, then inserted into a bacterial cloning vector by (A3600, Promega).

Cell lines, transfections, and small molecules

293F were obtained from Thermo (A14528). SK-MEL-5 cells, Daudi cells, and NIH3T3 cells were obtained from ATCC (HTB 70, CCL-213, and CRL-1658, respectively). The HEK293 Alix$^{-/-}$ cell line was described previously(*3*), as was the 293F/CD63$^{-/-}$ cell line (*50*). The 293F/AP2M1$^{-/-}$ cell line, 293F/CD9$^{-/-/-}$ cell line, and 293F/SDCBP$^{-/-}$ cell line were generated in this report (see section below describing Cas9-mediated gene editing). Adherent cultures were grown in tissue culture plates in complete medium (DMEM, 10% fetal bovine serum, 1% penicillin/streptomycin) at 37°C, 90% humidity, and 5% CO_2. For suspension cultures of 293F and 293F-derived cell lines, cells were grown in Freestyle medium (Thermo) in Erlenmeyer shaker flasks at 110 rpm, 37°C, 90% humidity, and 8% CO_2. DNA transfections were performed using Lipofectamine 3000 according to the manufacturer's instructions. Zeocin was used at 200 ug/mL. Puromycin was used at 3 ug/mL. Doxycycline was used at 10 ng/mL. Latrunculin A was used at 1 uM. Bafilomycin A was used at 100 nM.

To create the doxycycline-inducible Tet-on cell lines (i.e. FtetZ, 3TetZ, HtetZ/Alix$^{-/-}$, FtetZ/CD63$^{-/-}$, and FtetZ/CD9$^{-/-/-}$), the parental cell lines (293F, NIH3T3, HEK293/Alix$^{-/-}$, 293F/CD63$^{-/-}$, and 293F/CD9$^{-/-/-}$, respectively) were transfected with pJM1463 using Lipofectamine 3000 (Thermo). Two days later, the transfected cell populations were placed in zeocin-containing media. The culture medium was changed every 3-4 days for 7-12 days to select for zeocin-resistant cells. The thousands of surviving single cell clones from each transfection were then pooled to generate a single polyclonal Tet-on derivative of each parental cell line.

To create the cell lines that express the syntenin proteins, FtetZ, 3TetZ, and HtetZ/Alix$^{-/-}$ cells were transfected with pYA128, YA129, and pYA130. Two days later the cells were placed in puromycin-containing media, followed by selection of puromycin-resistant clones and pooling of all clones to create polyclonal cell lines designed for the doxycycline-induced expression of syntenin proteins. To create the cell lines that express CD9 proteins, FtetZ/CD9$^{-/-/-}$ cells were transfected with pCG606, pCG732, pCG733, pCG734, and pCG607. Two days later the cells were placed in hygromycin-containing media, followed by selection of hygromycin-resistant clones and pooling of all clones to create polyclonal cell lines designed for the doxycycline-induced expression of CD9 proteins. To create the cell lines that express CD63 proteins, FtetZ/CD63$^{-/-}$ cells were transfected with pCG602, pMG9, pCG604, and pMG10. Two days later the cells were placed in hygromycin-containing media, followed by selection of hygromycin-resistant clones and pooling of all clones to create polyclonal cell lines designed for the doxycycline-induced expression of CD63 proteins.

sEV preparation

For suspension cell cultures, cells were seeded into 30 ml of Freestyle medium at a density of 1 x 10^6 cells per ml and grown for 48-72 hours, with shaking. Culture media was collected and cells and cell debris were removed by centrifugation at 5,000 *g* at 4ºC for 15 minutes and by passage of the resulting supernatant through a 200 nm pore size diameter filtration unit. To collect sEVs by size exclusion chromatography and filtration, the 200 nm filtrate was concentrated ~100-fold by centrifugal flow filtration across a 100 kDa pore size diameter filter (Centricon-70, MilliporeSigma), followed by purification by size exclusion chromatography using qEV nano columns (Izon Sciences).

For adherent cell cultures, 6 million cells were seeded onto 150 mm dishes in 30 ml of complete medium, allowed to adhere to the plates overnight, then incubated for three days in complete medium. Culture media was collected and cells and cell debris were removed by centrifugation at 5,000 *g* at 4ºC for 15 minutes and by passage of the resulting supernatant through a 200 nm pore size diameter filtration unit. The sEVs were then collected by differential centrifugation, supernatants were spun for 30 minutes at 10,000 x *g*, spun a second time for 30 minutes at 10,000 x *g*, then spun at 100,000 *g* for 2 hours, all at 4ºC. The supernatant was discarded and the sEV pellet was resuspended for further analysis.

Immunoblot

Cells were lysed in Laemmli/SDS-PAGE sample buffer lacking reducing agent. Samples were either maintained in reducing agent-free sample buffer or adjusted to 5% ß-mercaptoethanol, then heated to 100ºC for 10 minutes, spun at 13,000 x g for 2 minutes to eliminate insoluble material, then separated by SDS-PAGE and processed for immunoblot as previously described using antibodies specific for human CD63 (NBP2-32830, NOVUS), mouse CD63 (NVG-2, Biolegend), CD9 (312102, Biolegend), CD81 (555675, BD Biosciences), Hsp90 (sc-13119, Santa Cruz Biotechnology), syntenin (PA5-76618, Thermo) AP2M1 (68196, Cell Signaling Technologies), Lamp1 (H4A3, Thermo), and Lamp2 (H4B4, Thermo). HRP-conjugated secondary antibodies were from Jackson ImmunoResearch.

qRT-PCR

Total RNA was isolated using Quick-RNA Microprep Kit (Zymo Research). RNA was converted to single stranded cDNA by reverse-transcription using the High-Capacity RNA-to-cDNA Kit (Applied Biosystems). qPCR analysis was performed using SYBR Green master mix (Bio-Rad) and the CFX96 Real-Time PCR Detection System (Bio-Rad), with gene-specific primers for our codon optimized syntenin transgene (5′- GGCTCAAGTCTATTGATAATGGC-3′ and 5′-CCTTATCACTGGACCAACC-3′), our CD9 transgene (5′-GAAATGTATTAAATATCTTCTGTTCGGTTT-3′ and 5′-CCGGCACCGATAAGTATATAAAC-3′) and control primers for human 18S rRNA (5′-CGGCGACGACCCATTCGAAC-3′ and 5′-GAATCGAACCCTGATTCCCCGTC-3′). Data was analyzed with ΔΔCT Method.

Flow cytometry and fluorescence activated cell sorting

Cells were released by trypsinization (TrypLE, Thermo) and cell clumps were removed using a cell-strainer (Falcon Cat#352235). Approximately 500,000 cells were then concentrated by a brief spin at 400 x *g* for 5 minutes and resuspended in 100 uL of 4ºC FACS buffer (1% FBS in PBS) containing 2 uL of FITC-conjugated anti-CD63 (clone H5C6), 2 uL APC conjugated anti-CD9 (clone H19a), 2 uL PE conjugated anti-CD81 (clone 5A6), or 2 uL PerCP conjugated anti-Lamp1 (clone H4A3) and 2 uL PE conjugated anti-Lamp2 (clone H4B4), all from Biolegend, for 30 min with gentle mixing every 10 min. Cells were washed 3 times with 1 mL of 4ºC FACS buffer, with cells recovered by 400 x *g* spin for 4 min at 4°C. After the final wash, cells were resuspended in FACS buffer with 0.5ug/ml DAPI, and analyzed using CytoFLEX S flow cytometer (Beckman Coulter). Flow cytometry histograms were generated using FlowJo (v10.8.1). For separation by FACS, labeled cells were sorted into single cells in a 96 well plate, on the basis of high or low cell surface labeling for CD63 or CD9.

Cas9-medited gene editing

To create the 293F/AP2M1$^{-/-}$ cell line, we transfected 293F cells with a mixture of Cas9 protein (A36498, Thermo) and an AP2M1-targeting single guide RNA (sgRNA; target sequence of 5'-ACGTTAAGCGGTCCAACATT-3') using lipofectamine CRISPRMAX (Thermo). Cells were cultured for several days, then seeded into wells of into 96 well plates at one cell per well. Single cell clones (SCCs) were expanded, genomic DNA (gDNA) was extracted from each clone, and each gDNA was interrogated by PCR using AP2M1 gene-specific primers. PCR products were ligated into the pGEM®-T vector using a TA cloning kit (A3600, Promega), transformed into *E. coli*, and 8 or more clones from each ligation were sequenced in their entirety. The 293F/AP2M1$^{-/-}$ cell line carried for further analysis carried one allele with a 198 bp deletion and one allele with a = 1 codon deletion at a conserved position (Ile63Δ) of the AP2M1 protein (***Fig. S5***).

A similar procedure was used to generate the 293F/CD9$^{-/-/-}$ cell line. 293F cells were transfected with a mixture of Cas9 protein (A36498, Thermo) and a sgRNA guide RNA (target sequence of 5'-ATTCGCCATTGAAATAGCTG-3') using lipofectamine CRISPRMAX (Thermo). Cells were cultured for several days, trypsinized, and seeded into wells of into 96 well plates at one cell per well. Single cell clones were expanded, genomic DNA (gDNA) was extracted from each clone, and each gDNA was interrogated by PCR using CD9 gene-specific primers. PCR products were ligated into the pGEM®-T vector using a TA cloning kit (A3600, Promega), transformed into *E. coli*, and 24 or more clones from each ligation were sequenced in their entirety. All gDNA amplification products from 293F/CD9$^{-/-/-}$ cell lines carried up to three different sequences, indicating that 293F cells carry three CD9 alleles. The cell line used for further experimentation carried one CD9 allele with a 4 bp deletion and two CD9 alleles with the same 8bp deletion. (***Fig. S8***).

The 293F/SDCBP$^{-/-}$ cell line was created by transfecting 293F cells with the plasmid pJM1087 then selecting for puromycin-resistant cell clones. After 7 days in selection, surviving cells were pooled, with EGFP-positive cells separated by FACS into individual wells of a 96 well plate. The emergent SCCs were expanded and 10 were interrogated by immunoblot using antibodies specific for syntenin, revealing that all 10 lacked detectable level of syntenin protein. We then extracted gDNA from these clones and interrogated each gDNA by PCR using primers flanking both gRNA target sites in the SDCBP gene. The 293F/SDCBP$^{-/-}$ cell line selected carried deletions between the two target sites in coding exons 2 and 3 on both of its SDCBP alleles rendering both functionally null. To delete the Cas9-EGFP-HSVtk-PuroR ORF, this cell line was transfected with a Cre recombinase expression vector, grown for 10 days in CM lacking antibiotics, then seeded at various densities into CM containing ganciclovir to eliminate any HSVtk-expressing cells. After growth and selection for two weeks in ganciclovir-containing medium, the resulting cell clones were pooled and examined by flow cytometry, revealing that all cells in the population were EGFP-negative. Furthermore, exposure of these cells to puromycin confirmed that all of the cells in the ganciclovir-resistant population had also reverted to puromycin sensitivity, and were therefore likely no longer expressing Cas9.

Endocytosis assay and confocal fluorescence microscopy

Cells were grown overnight on poly-D-lysine-coated coverglasses in CM, then transferred to pre-chilled 4ºC CM. Cells were washed in 4ºC PBS, then incubated for 30 minutes at 4ºC with pre-chilled 4ºC PBS (200 uL) containing 4 uL FITC-conjugated anti-CD63 (clone H5C6, Biolegend) and 4 uL APC conjugated anti-CD9 (clone H19a, Biolegend). Excess antibody was removed by two washes with 4ºC PBS. Cells were then fixed immediately or transferred to CM at 37ºC and incubated for 30 minutes at 37ºC. Fixation was with 3.7% formaldehyde in PBS for 20 minutes. Cells were then incubated with DAPI to stain the nucleus, and then examined by confocal fluorescence microscopy and imaged to assess the subcellular distribution of plasma membrane-labeled CD63 and CD9. Confocal fluorescence microscopy was performed using a Zeiss LSM880 microscope with gallium-arsenide phosphide (GaAsP) detectors and a 63x/1.4na Plan-Apochromat objective. Images were assembled into figures using ImageJ and Adobe Illustrator.

SPIR-IFM analysis

Exosomes were purified by filtration and size exclusion chromatography, then further purified by affinity capture on anti-CD81 or anti-CD9 antibodies that had been immobilized on SPIR imaging chips (Unchained Labs). Bound exosomes were then stained using CF-647 conjugate of a mouse anti-human CD63 monoclonal antibody (Unchained Labs) and imaged using an Exoview R200 imaging platform (Unchained Labs).

qSMLM analysis

25 mm diameter coverslips #1.5H (Thermo Fischer Scientific, Cat# NC9560650; Waltham, MA, USA) were functionalized with N-hydroxysuccinimide (NHS) groups, followed by covalent attachment of monoclonal antibodies that bind to epitopes in the ectodomain of human CD81 and human CD9. FtetZ cells and FtetZ::syntenin cells were grown in Freestyle media containing doxycycline, followed by collection of their exosomes by concentrating filtration and size exclusion chromatography. The resulting exosome preparations were diluted in PBS containing 0.025% Tween 20 (1:50) to a final volume of 80 uL and placed on the surface of antibody-coated coverslips at room temperature overnight in a humidified chamber. Coverslips were then washed with PBS containing 0.025% Tween 20 and EVs were labeled with a cocktail of AF647-labeled antibodies specific for human CD63 (Novus Biologicals Cat. No. NBP2-42225 Centennial, CO, USA) and CF568-labeled antibodies specific for human CD9 (BioLegend, Cat. No. 312102, San Diego, CA,

USA) and human CD81 (BioLegend, Cat. No. 349502, San Diego, CA, USA). All antibodies were fluorescently labeled as described previously at a molar ratio of ~1 (*74*)). Samples were fixed and stored as described previously(*75, 76*).

For imaging, coverslips were placed in Attofluor cell chambers (Thermo Fisher Scientific, Cat. No. A7816) loaded with direct stochastic optical reconstruction microscopy (dSTORM) imaging buffer(*77*). N-STORM super-resolution microscope (Nikon Instruments; Melville, NY, USA) was used for SMLM imaging using 561 nm and 640 nm lasers, respectively, using microscope components described previously(*78*). Images were acquired using NIS-Elements software (Nikon Instruments). SMLM images were processed using N-STORM Offline Analysis Module of the NIS-Elements software to localize peaks as described before(*75*). The localization data were analyzed with the Nanometrix software (version 1.0.4.61; Nanometrix Ltd, Oxford, UK) using a density-based spatial clustering of applications with noise (DBSCAN) algorithm. Prior to cluster analysis, the detected 640 nm and 561 nm channel localizations were aligned using the Uniform Dual Channel Alignment tool of Nanometrix. The DBSCAN-based cluster identification was performed at a neighbor search radius of 30 nm and minimum points per cluster of 30 as analysis conditions. Post-processing of the detected cluster data, including concatenation and filtering, was performed using Matlab (version R2022a; MathWorks; Natick, MA, USA). Clusters were identified as EVs considering the following constraints. In the case of the 647 nm channel, the minimum and maximum number of localizations per cluster was set to 30 and 3000, as well as the minimum and maximum diameter was set to 20 nm and 400 nm, respectively. In the case of the 561 nm channel, the minimum and maximum number of localizations per cluster was set to 40 and 3200, as well as the minimum and maximum diameter was set to 30 nm and 400 nm, respectively. Colocalized (CD63+, CD81/CD9+) EVs were identified as overlapping clusters detected in the 640 nm and 561 nm channel. The number of tetraspanin molecules per exosome was calculated using an average of 15 (647 nm channel) and 16 (561 nm channel) localizations per single fluorescent tetraspanin antibody, as described before(*79*). Following EV identification, the EV count per region of interest (ROI), CD63 molecule count per EV, and EV diameter were further analyzed. To account for the difference in EV concentration across the samples, we normalized the number of detected CD63+, CD81/CD9+ and CD63-, CD81/CD9+ EVs by the total number of CD81/CD9+ EVs. Statistical significances in the normalized EV count per ROI data were determined using Brown-Forsythe and Welch ANOVA test. Statistical significance in the CD63 molecule count per EV and diameter data was assessed performing two-tailed Welch's t-test after logarithmic transformation. Statistical analysis and graph generation were performed in GraphPad Prism (version 9.5.1; GraphPad, San Diego, CA, USA).

Analysis of RNAseq data

The web tool 'AnalyzeR' was used to analysis RNA expression data of CD63 and SDCBP in >230,00 distinct samples that had been examined from normal and malignant human tissues, as previously described(*80*).

References

1. J. M. Escola, M. J. Kleijmeer, W. Stoorvogel, J. M. Griffith, O. Yoshie, H. J. Geuze, Selective enrichment of tetraspan proteins on the internal vesicles of multivesicular endosomes and on exosomes secreted by human B-lymphocytes. *J Biol Chem* **273**, 20121-20127 (1998).
2. C. Thery, A. Regnault, J. Garin, J. Wolfers, L. Zitvogel, P. Ricciardi-Castagnoli, G. Raposo, S. Amigorena, Molecular characterization of dendritic cell-derived exosomes. Selective accumulation of the heat shock protein hsc73. *J Cell Biol* **147**, 599-610 (1999).
3. F. K. Fordjour, C. Guo, Y. Ai, G. G. Daaboul, S. J. Gould, A shared, stochastic pathway mediates exosome protein budding along plasma and endosome membranes. *J Biol Chem*, 102394 (2022).
4. F. G. Kugeratski, K. Hodge, S. Lilla, K. M. McAndrews, X. Zhou, R. F. Hwang, S. Zanivan, R. Kalluri, Quantitative proteomics identifies the core proteome of exosomes with syntenin-1 as the highest abundant protein and a putative universal biomarker. *Nat Cell Biol* **23**, 631-641 (2021).
5. D. M. Pegtel, S. J. Gould, Exosomes. *Annu Rev Biochem* **88**, 487-514 (2019).
6. L. Li, K. Piontek, M. Ishida, M. Fausther, J. A. Dranoff, R. Fu, E. Mezey, S. J. Gould, F. K. Fordjour, S. J. Meltzer, A. E. Sirica, F. M. Selaru, Extracellular vesicles carry microRNA-195 to intrahepatic cholangiocarcinoma and improve survival in a rat model. *Hepatology* **65**, 501-514 (2017).
7. S. Kamerkar, V. S. LeBleu, H. Sugimoto, S. Yang, C. F. Ruivo, S. A. Melo, J. J. Lee, R. Kalluri, Exosomes facilitate therapeutic targeting of oncogenic KRAS in pancreatic cancer. *Nature* **546**, 498-503 (2017).
8. K. Dooley, R. E. McConnell, K. Xu, N. D. Lewis, S. Haupt, M. R. Youniss, S. Martin, C. L. Sia, C. McCoy, R. J. Moniz, O. Burenkova, J. Sanchez-Salazar, S. C. Jang, B. Choi, R. A. Harrison, D. Houde, D. Burzyn, C. Leng, K. Kirwin, N. L. Ross, J. D. Finn, L. Gaidukov, K. D. Economides, S. Estes, J. E. Thornton, J. D. Kulman, S. Sathyanarayanan, D. E. Williams, A versatile platform for generating engineered extracellular vesicles with defined therapeutic properties. *Mol Ther* **29**, 1729-1743 (2021).
9. S. J. Tsai, N. A. Atai, M. Cacciottolo, J. Nice, A. Salehi, C. Guo, A. Sedgwick, S. Kanagavelu, S. J. Gould, Exosome-mediated mRNA Delivery in vivo is safe and can be used to induce SARS-CoV-2 immunity. *J Biol Chem*, 101266 (2021).
10. M. Mathieu, N. Nevo, M. Jouve, J. I. Valenzuela, M. Maurin, F. J. Verweij, R. Palmulli, D. Lankar, F. Dingli, D. Loew, E. Rubinstein, G. Boncompain, F. Perez, C. Thery, Specificities of exosome versus small ectosome secretion revealed by live intracellular tracking of CD63 and CD9. *Nat Commun* **12**, 4389 (2021).
11. W. Stoorvogel, Resolving sorting mechanisms into exosomes. *Cell Res* **25**, 531-532 (2015).
12. R. Kashyap, M. Balzano, B. Lechat, K. Lambaerts, A. L. Egea-Jimenez, F. Lembo, J. Fares, S. Meeussen, S. Kugler, A. Roebroek, G. David, P. Zimmermann, Syntenin-knock out reduces exosome turnover and viral transduction. *Sci Rep* **11**, 4083 (2021).
13. M. Mathieu, L. Martin-Jaular, G. Lavieu, C. Thery, Specificities of secretion and uptake of exosomes and other extracellular vesicles for cell-to-cell communication. *Nat Cell Biol* **21**, 9-17 (2019).
14. A. Bobrie, M. Colombo, G. Raposo, C. Thery, Exosome secretion: molecular mechanisms and roles in immune responses. *Traffic* **12**, 1659-1668 (2011).
15. C. Thery, M. Ostrowski, E. Segura, Membrane vesicles as conveyors of immune responses. *Nat Rev Immunol* **9**, 581-593 (2009).

16. W. Stoorvogel, M. J. Kleijmeer, H. J. Geuze, G. Raposo, The biogenesis and functions of exosomes. *Traffic* **3**, 321-330 (2002).
17. C. Thery, L. Zitvogel, S. Amigorena, Exosomes: composition, biogenesis and function. *Nat Rev Immunol* **2**, 569-579 (2002).
18. G. Raposo, W. Stoorvogel, Extracellular vesicles: exosomes, microvesicles, and friends. *J Cell Biol* **200**, 373-383 (2013).
19. M. Mathieu, N. Nevo, M. Jouve, J. I. Valenzuela, M. Maurin, F. J. Verweij, R. Palmulli, D. Lankar, F. Dingli, D. Loew, E. Rubinstein, G. Boncompain, F. Perez, C. Thery, Specificities of exosome versus small ectosome secretion revealed by live intracellular tracking of CD63 and CD9. *bioRxiv*, (2020).
20. M. F. Baietti, Z. Zhang, E. Mortier, A. Melchior, G. Degeest, A. Geeraerts, Y. Ivarsson, F. Depoortere, C. Coomans, E. Vermeiren, P. Zimmermann, G. David, Syndecan-syntenin-ALIX regulates the biogenesis of exosomes. *Nat Cell Biol* **14**, 677-685 (2012).
21. J. Larios, V. Mercier, A. Roux, J. Gruenberg, ALIX- and ESCRT-III-dependent sorting of tetraspanins to exosomes. *J Cell Biol* **219**, (2020).
22. K. W. Witwer, C. Thery, Extracellular vesicles or exosomes? On primacy, precision, and popularity influencing a choice of nomenclature. *J Extracell Vesicles* **8**, 1648167 (2019).
23. N. Latysheva, G. Muratov, S. Rajesh, M. Padgett, N. A. Hotchin, M. Overduin, F. Berditchevski, Syntenin-1 is a new component of tetraspanin-enriched microdomains: mechanisms and consequences of the interaction of syntenin-1 with CD63. *Mol Cell Biol* **26**, 7707-7718 (2006).
24. J. Codina, J. Li, T. D. Dubose, Jr., CD63 interacts with the carboxy terminus of the colonic H+-K+-ATPase to decrease [corrected] plasma membrane localization and 86Rb+ uptake. *Am J Physiol Cell Physiol* **288**, C1279-1286 (2005).
25. A. Duffield, E. J. Kamsteeg, A. N. Brown, P. Pagel, M. J. Caplan, The tetraspanin CD63 enhances the internalization of the H,K-ATPase beta-subunit. *Proc Natl Acad Sci U S A* **100**, 15560-15565 (2003).
26. M. S. Pols, J. Klumperman, Trafficking and function of the tetraspanin CD63. *Exp Cell Res* **315**, 1584-1592 (2009).
27. T. Takino, H. Miyamori, N. Kawaguchi, T. Uekita, M. Seiki, H. Sato, Tetraspanin CD63 promotes targeting and lysosomal proteolysis of membrane-type 1 matrix metalloproteinase. *Biochem Biophys Res Commun* **304**, 160-166 (2003).
28. N. Yoshida, D. Kitayama, M. Arima, A. Sakamoto, A. Inamine, H. Watanabe-Takano, M. Hatano, T. Koike, T. Tokuhisa, CXCR4 expression on activated B cells is downregulated by CD63 and IL-21. *J Immunol* **186**, 2800-2808 (2011).
29. L. Grassel, L. A. Fast, K. D. Scheffer, F. Boukhallouk, G. A. Spoden, S. Tenzer, K. Boller, R. Bago, S. Rajesh, M. Overduin, F. Berditchevski, L. Florin, The CD63-Syntenin-1 Complex Controls Post-Endocytic Trafficking of Oncogenic Human Papillomaviruses. *Sci Rep* **6**, 32337 (2016).
30. Y. Fang, N. Wu, X. Gan, W. Yan, J. C. Morrell, S. J. Gould, Higher-order oligomerization targets plasma membrane proteins and HIV gag to exosomes. *PLoS Biol* **5**, e158 (2007).
31. A. M. Booth, Y. Fang, J. K. Fallon, J. M. Yang, J. E. Hildreth, S. J. Gould, Exosomes and HIV Gag bud from endosome-like domains of the T cell plasma membrane. *J Cell Biol* **172**, 923-935 (2006).
32. B. Shen, N. Wu, J. M. Yang, S. J. Gould, Protein targeting to exosomes/microvesicles by plasma membrane anchors. *J Biol Chem* **286**, 14383-14395 (2011).
33. F. K. D. Fordjour, G. G., S. J. Gould, A shared pathway of exosome biogenesis operates at plasma and endosome membranes. *BiorXiv*, 1-42 (2019). doi: https://doi.org/10.1101/545228

34. M. S. Marks, H. Ohno, T. Kirchnausen, J. S. Bonracino, Protein sorting by tyrosine-based signals: adapting to the Ys and wherefores. *Trends Cell Biol* **7**, 124-128 (1997).
35. H. Ohno, J. Stewart, M. C. Fournier, H. Bosshart, I. Rhee, S. Miyatake, T. Saito, A. Gallusser, T. Kirchhausen, J. S. Bonifacino, Interaction of tyrosine-based sorting signals with clathrin-associated proteins. *Science* **269**, 1872-1875 (1995).
36. G. G. Daaboul, D. S. Freedman, S. M. Scherr, E. Carter, A. Rosca, D. Bernstein, C. E. Mire, K. N. Agans, T. Hoenen, T. W. Geisbert, M. S. Unlu, J. H. Connor, Enhanced light microscopy visualization of virus particles from Zika virus to filamentous ebolaviruses. *PLoS One* **12**, e0179728 (2017).
37. W. Matsui, T. Kirchhausen, Stabilization of clathrin coats by the core of the clathrin-associated protein complex AP-2. *Biochemistry* **29**, 10791-10798 (1990).
38. T. Braulke, J. S. Bonifacino, Sorting of lysosomal proteins. *Biochim Biophys Acta* **1793**, 605-614 (2009).
39. L. M. Traub, J. S. Bonifacino, Cargo recognition in clathrin-mediated endocytosis. *Cold Spring Harb Perspect Biol* **5**, a016790 (2013).
40. M. Akamatsu, R. Vasan, D. Serwas, M. A. Ferrin, P. Rangamani, D. G. Drubin, Principles of self-organization and load adaptation by the actin cytoskeleton during clathrin-mediated endocytosis. *Elife* **9**, (2020).
41. C. Hinze, E. Boucrot, Local actin polymerization during endocytic carrier formation. *Biochem Soc Trans* **46**, 565-576 (2018).
42. M. Jin, C. Shirazinejad, B. Wang, A. Yan, J. Schoneberg, S. Upadhyayula, K. Xu, D. G. Drubin, Branched actin networks are organized for asymmetric force production during clathrin-mediated endocytosis in mammalian cells. *Nat Commun* **13**, 3578 (2022).
43. C. Lamaze, L. M. Fujimoto, H. L. Yin, S. L. Schmid, The actin cytoskeleton is required for receptor-mediated endocytosis in mammalian cells. *J Biol Chem* **272**, 20332-20335 (1997).
44. D. Yarar, C. M. Waterman-Storer, S. L. Schmid, A dynamic actin cytoskeleton functions at multiple stages of clathrin-mediated endocytosis. *Mol Biol Cell* **16**, 964-975 (2005).
45. S. M. Migliano, E. M. Wenzel, H. Stenmark, Biophysical and molecular mechanisms of ESCRT functions, and their implications for disease. *Curr Opin Cell Biol* **75**, 102062 (2022).
46. M. Vietri, M. Radulovic, H. Stenmark, The many functions of ESCRTs. *Nat Rev Mol Cell Biol* **21**, 25-42 (2020).
47. R. A. Warren, F. A. Green, C. A. Enns, Saturation of the endocytic pathway for the transferrin receptor does not affect the endocytosis of the epidermal growth factor receptor. *J Biol Chem* **272**, 2116-2121 (1997).
48. R. A. Warren, F. A. Green, P. E. Stenberg, C. A. Enns, Distinct saturable pathways for the endocytosis of different tyrosine motifs. *J Biol Chem* **273**, 17056-17063 (1998).
49. H. S. Wiley, Anomalous binding of epidermal growth factor to A431 cells is due to the effect of high receptor densities and a saturable endocytic system. *J Cell Biol* **107**, 801-810 (1988).
50. S. J. Tsai, Y. Ai, C. Guo, S. J. Gould, Degron-tagging of BleoR and other antibiotic-resistance genes selects for higher expression of linked transgenes and improved exosome engineering. *J Biol Chem*, 101846 (2022).
51. A. Digre, C. Lindskog, The human protein atlas-Integrated omics for single cell mapping of the human proteome. *Protein Sci* **32**, e4562 (2023).
52. X. Gan, S. J. Gould, Identification of an inhibitory budding signal that blocks the release of HIV particles and exosome/microvesicle proteins. *Mol Biol Cell* **22**, 817-830 (2011).
53. S. J. Gould, A. M. Booth, J. E. Hildreth, The Trojan exosome hypothesis. *Proc Natl Acad Sci U S A* **100**, 10592-10597 (2003).

54. C. Guo, F. K. Fordjour, S. J. Tsai, J. C. Morrell, S. J. Gould, Choice of selectable marker affects recombinant protein expression in cells and exosomes. *J Biol Chem*, 100838 (2021).
55. B. Shen, Y. Fang, N. Wu, S. J. Gould, Biogenesis of the posterior pole is mediated by the exosome/microvesicle protein-sorting pathway. *J Biol Chem* **286**, 44162-44176 (2011).
56. J. M. Yang, S. J. Gould, The cis-acting signals that target proteins to exosomes and microvesicles. *Biochem Soc Trans* **41**, 277-282 (2013).
57. J. K. Williams, J. M. Ngo, I. M. Lehman, R. Schekman, Annexin A6 mediates calcium-dependent exosome secretion during plasma membrane repair. *Elife* **12**, (2023).
58. K. Sagini, S. Buratta, F. Delo, R. M. Pellegrino, S. Giovagnoli, L. Urbanelli, C. Emiliani, Drug-Induced Lysosomal Impairment Is Associated with the Release of Extracellular Vesicles Carrying Autophagy Markers. *Int J Mol Sci* **22**, (2021).
59. T. A. Solvik, T. A. Nguyen, Y. H. Tony Lin, T. Marsh, E. J. Huang, A. P. Wiita, J. Debnath, A. M. Leidal, Secretory autophagy maintains proteostasis upon lysosome inhibition. *J Cell Biol* **221**, (2022).
60. T. Mitsunari, F. Nakatsu, N. Shioda, P. E. Love, A. Grinberg, J. S. Bonifacino, H. Ohno, Clathrin adaptor AP-2 is essential for early embryonal development. *Mol Cell Biol* **25**, 9318-9323 (2005).
61. A. Yoshimura, M. Kawamata, Y. Yoshioka, T. Katsuda, H. Kikuchi, Y. Nagai, N. Adachi, T. Numakawa, H. Kunugi, T. Ochiya, Y. Tamai, Generation of a novel transgenic rat model for tracing extracellular vesicles in body fluids. *Sci Rep* **6**, 31172 (2016).
62. A. Yoshimura, N. Adachi, H. Matsuno, M. Kawamata, Y. Yoshioka, H. Kikuchi, H. Odaka, T. Numakawa, H. Kunugi, T. Ochiya, Y. Tamai, The Sox2 promoter-driven CD63-GFP transgenic rat model allows tracking of neural stem cell-derived extracellular vesicles. *Dis Model Mech* **11**, (2018).
63. J. V. McCann, S. R. Bischoff, Y. Zhang, D. O. Cowley, V. Sanchez-Gonzalez, G. D. Daaboul, A. C. Dudley, Reporter mice for isolating and auditing cell type-specific extracellular vesicles in vivo. *Genesis* **58**, e23369 (2020).
64. F. J. Verweij, C. Revenu, G. Arras, F. Dingli, D. Loew, D. M. Pegtel, G. Follain, G. Allio, J. G. Goetz, P. Zimmermann, P. Herbomel, F. Del Bene, G. Raposo, G. van Niel, Live Tracking of Inter-organ Communication by Endogenous Exosomes In Vivo. *Dev Cell* **48**, 573-589 e574 (2019).
65. Y. Men, J. Yelick, S. Jin, Y. Tian, M. S. R. Chiang, H. Higashimori, E. Brown, R. Jarvis, Y. Yang, Exosome reporter mice reveal the involvement of exosomes in mediating neuron to astroglia communication in the CNS. *Nat Commun* **10**, 4136 (2019).
66. B. H. Sung, A. von Lersner, J. Guerrero, E. S. Krystofiak, D. Inman, R. Pelletier, A. Zijlstra, S. M. Ponik, A. M. Weaver, A live cell reporter of exosome secretion and uptake reveals pathfinding behavior of migrating cells. *Nat Commun* **11**, 2092 (2020).
67. J. Yang, F. Wei, C. Schafer, D. T. Wong, Detection of tumor cell-specific mRNA and protein in exosome-like microvesicles from blood and saliva. *PLoS One* **9**, e110641 (2014).
68. Y. Matsumoto, M. Kano, Y. Akutsu, N. Hanari, I. Hoshino, K. Murakami, A. Usui, H. Suito, M. Takahashi, R. Otsuka, H. Xin, A. Komatsu, K. Iida, H. Matsubara, Quantification of plasma exosome is a potential prognostic marker for esophageal squamous cell carcinoma. *Oncol Rep* **36**, 2535-2543 (2016).
69. L. Sadovska, E. Zandberga, K. Sagini, K. Jekabsons, U. Riekstina, Z. Kalnina, A. Llorente, A. Line, A novel 3D heterotypic spheroid model for studying extracellular vesicle-mediated tumour and immune cell communication. *Biochem Biophys Res Commun* **495**, 1930-1935 (2018).
70. T. Satake, A. Suetsugu, M. Nakamura, T. Kunisada, S. Saji, H. Moriwaki, M. Shimizu, R. M. Hoffman, Color-coded Imaging of the Fate of Cancer-cell-derived Exosomes During

Pancreatic Cancer Metastases in a Nude-mouse Model. *Anticancer Res* **39**, 4055-4060 (2019).

71. F. J. Verweij, M. P. Bebelman, C. R. Jimenez, J. J. Garcia-Vallejo, H. Janssen, J. Neefjes, J. C. Knol, R. de Goeij-de Haas, S. R. Piersma, S. R. Baglio, M. Verhage, J. M. Middeldorp, A. Zomer, J. van Rheenen, M. G. Coppolino, I. Hurbain, G. Raposo, M. J. Smit, R. F. G. Toonen, G. van Niel, D. M. Pegtel, Quantifying exosome secretion from single cells reveals a modulatory role for GPCR signaling. *J Cell Biol* **217**, 1129-1142 (2018).
72. S. J. Gould, G. Raposo, As we wait: coping with an imperfect nomenclature for extracellular vesicles. *J Extracell Vesicles* **2**, (2013).
73. E. Cocucci, J. Meldolesi, Ectosomes. *Curr Biol* **21**, R940-941 (2011).
74. S. J. Tobin, D. L. Wakefield, V. Jones, X. Liu, D. Schmolze, T. Jovanovic-Talisman, Single molecule localization microscopy coupled with touch preparation for the quantification of trastuzumab-bound HER2. *Sci Rep* **8**, 15154 (2018).
75. K. M. Lennon, A. Saftics, S. Abuelreich, P. Sahu, H. I. Lehmann, A. L. Maddox, R. Bagabas, J. L. Januzzi, K. Van Keuren-Jensen, R. Shah, S. Das, T. Jovanovic-Talisman, Cardiac troponin T in extracellular vesicles as a novel biomarker in human cardiovascular disease. *Clin Transl Med* **12**, e979 (2022).
76. K. M. Lennon, D. L. Wakefield, A. L. Maddox, M. S. Brehove, A. N. Willner, K. Garcia-Mansfield, B. Meechoovet, R. Reiman, E. Hutchins, M. M. Miller, A. Goel, P. Pirrotte, K. Van Keuren-Jensen, T. Jovanovic-Talisman, Single molecule characterization of individual extracellular vesicles from pancreatic cancer. *J Extracell Vesicles* **8**, 1685634 (2019).
77. G. T. Dempsey, J. C. Vaughan, K. H. Chen, M. Bates, X. Zhuang, Evaluation of fluorophores for optimal performance in localization-based super-resolution imaging. *Nat Methods* **8**, 1027-1036 (2011).
78. A. L. Maddox, M. S. Brehove, K. R. Eliato, A. Saftics, E. Romano, M. F. Press, J. Mortimer, V. Jones, D. Schmolze, V. L. Seewaldt, T. Jovanovic-Talisman, Molecular Assessment of HER2 to Identify Signatures Associated with Therapy Response in HER2-Positive Breast Cancer. *Cancers (Basel)* **14**, (2022).
79. O. Golfetto, D. L. Wakefield, E. E. Cacao, K. N. Avery, V. Kenyon, R. Jorand, S. J. Tobin, S. Biswas, J. Gutierrez, R. Clinton, Y. Ma, D. A. Horne, J. C. Williams, T. Jovanovic-Talisman, A Platform To Enhance Quantitative Single Molecule Localization Microscopy. *J Am Chem Soc* **140**, 12785-12797 (2018).
80. H. E. Miller, A. J. R. Bishop, Correlation AnalyzeR: functional predictions from gene co-expression correlations. *BMC Bioinformatics* **22**, 206 (2021).

Acknowledgments: The authors thank James Morrell for his outstanding technical assistance and to the many colleagues who provided feedback over the course of this project, especially Drs. Xandra Breakefield, Michael Caterina, Chulhee Choi, Saumya Das, Samir El-Andaloussi, Dhanu Gupta, Tijana Jovanovic-Talisman, Michiel Pegtel, Shang Jui Tsai, and Antje Zickler.

Funding: This work was supported by grants from the NIH (UG3 CA241687, R35 HL150807, UG3 TR002878) and institutional funds of Johns Hopkins University

Author contributions:
Conceptualization: YA, CG, MG-C, SJT, TJ-T, SJG
Methodology: YA, CG, MC-G, AS, TJ-T, SJG
Investigation: YA, CG, OS, SR, YD, SJG
Visualization: YA, CG, MG-C, AS, SJG
Funding acquisition: TJ-T, SJG
Project administration: TJ-T, SJG
Supervision: TJ-T, RL, SJG
Writing – original draft: SJG
Writing – review & editing: YA, CG, MG-C, TJ-T, SJG

Competing interests: Authors declare that they have no competing interests.

Data and materials availability: All data are available in the main text or the supplementary materials.

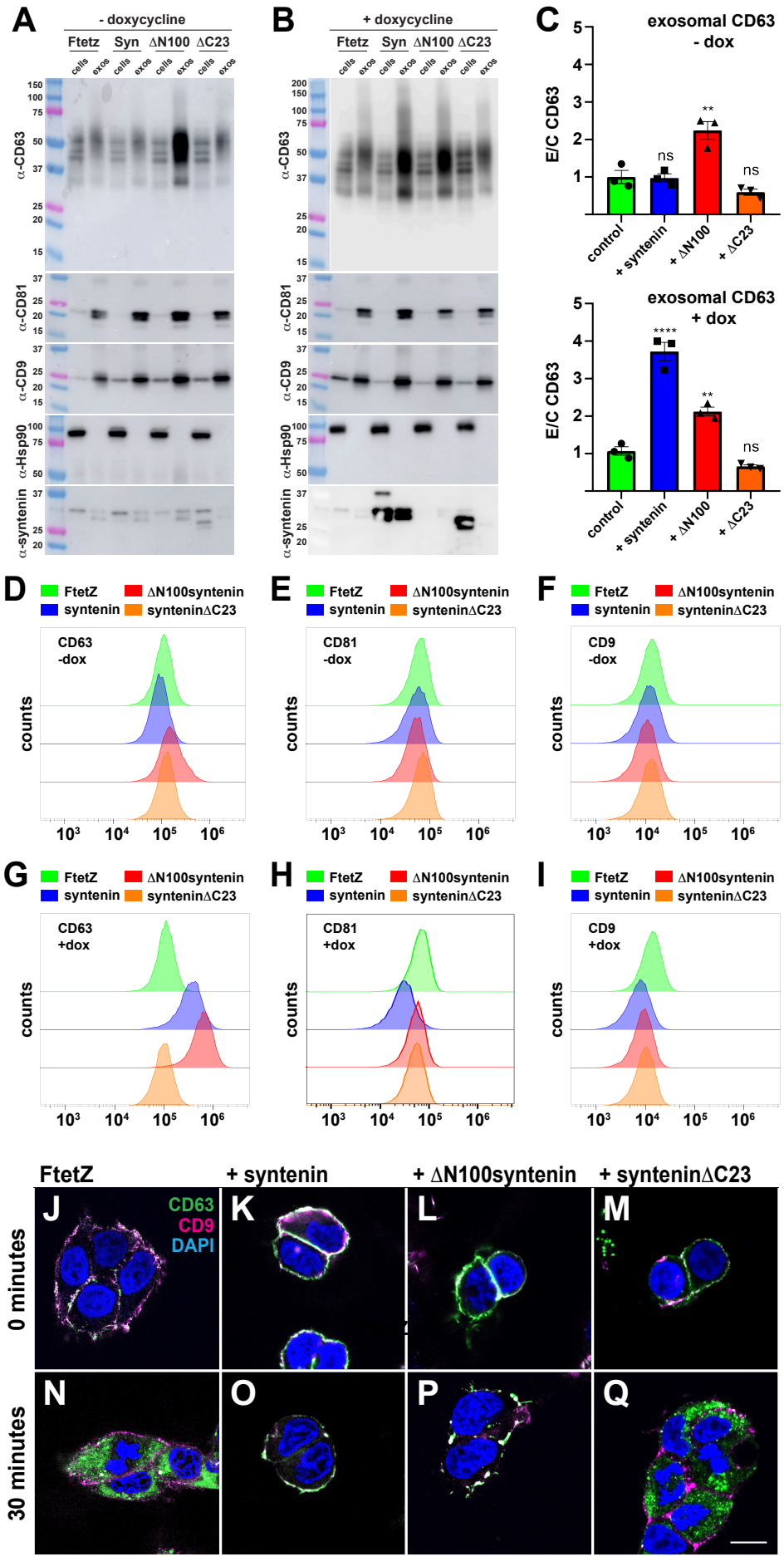
A
- doxycycline
Ftetz
Syn
ΔN100
ΔC23
cells
exos
α-CD63
α-CD81
α-CD9
α-Hsp90
α-syntenin
B
+ doxycycline
C
exosomal CD63
- dox
E/C CD63
ns
**
control
+ syntenin
+ ΔN100
+ ΔC23
exosomal CD63
+ dox
****
D
FtetZ
syntenin
ΔN100syntenin
syntenin ΔC23
CD63
-dox
counts
E
CD81
-dox
F
CD9
-dox
G
CD63
+dox
H
CD81
+dox
I
CD9
+dox
FtetZ
+ syntenin
+ ΔN100syntenin
+ syntenin ΔC23
0 minutes
30 minutes
J
CD63
CD9
DAPI
K
L
M
N
O
P
Q

Figure 1. Syntenin induces the exosomal secretion of CD63 by blocking CD63 endocytosis. Immunoblot analysis of cell and exosome lysates collected from FtetZ and FtetZ cells carrying TRE3G-regulated transgenes encoding (Syn) WT human syntenin, (ΔN100) ΔN100syntenin, or (ΔC23) synteninΔC23, grown in the (**A**) absence or (**B**) presence of doxycycline. Immunoblots were probed using antibodies specific for the exosome cargo proteins CD63, CD9, and CD81, the cytoplasmic protein Hsp90, and syntenin. The anti-syntenin antibody was raised against an N-terminal fragment and does not bind ΔN100syntenin. Similar results were observed in multiple trials (n = 4). (**C**) Bar graphs showing the mean exosome/cell ratio of CD63, +/- standard error of the mean (s.e.m.) in the experiments of A and B. Statistical significance was assessed by ANOVA, with ** denoting *p* value <0.01 and **** denoting a *p* value <0.0001. (**D-I**) Flow cytometry histograms of FtetZ and FtetZ cells carrying TRE3G-regulated transgenes encoding (Syn) WT human syntenin, (ΔN100) ΔN100syntenin, or (ΔC23) synteninΔC23, grown in the (D-F) absence or (G-I) presence of doxycycline, chilled and stained for the cell surface abundance of (D, G) CD63, (E, H) CD81, or (F, I) CD9. (**J-Q**) Confocal fluorescence microscopy of (J, N) FtetZ cells, and FtetZ cells carrying TRE3G-regulated transgenes encoding (K, O) syntenin, (L, P) ΔN100syntenin, or (M, Q) synteninΔC23 that had been chilled, incubated with fluorescently tagged antibodies specific for (green) CD63 and (pink) CD9, then warmed and then fixed and imaged after (J-M) 0 minutes at 37ºC or (N-Q) 30 minutes at 37ºC. Bar, 10 um. Data is from three independent trails.

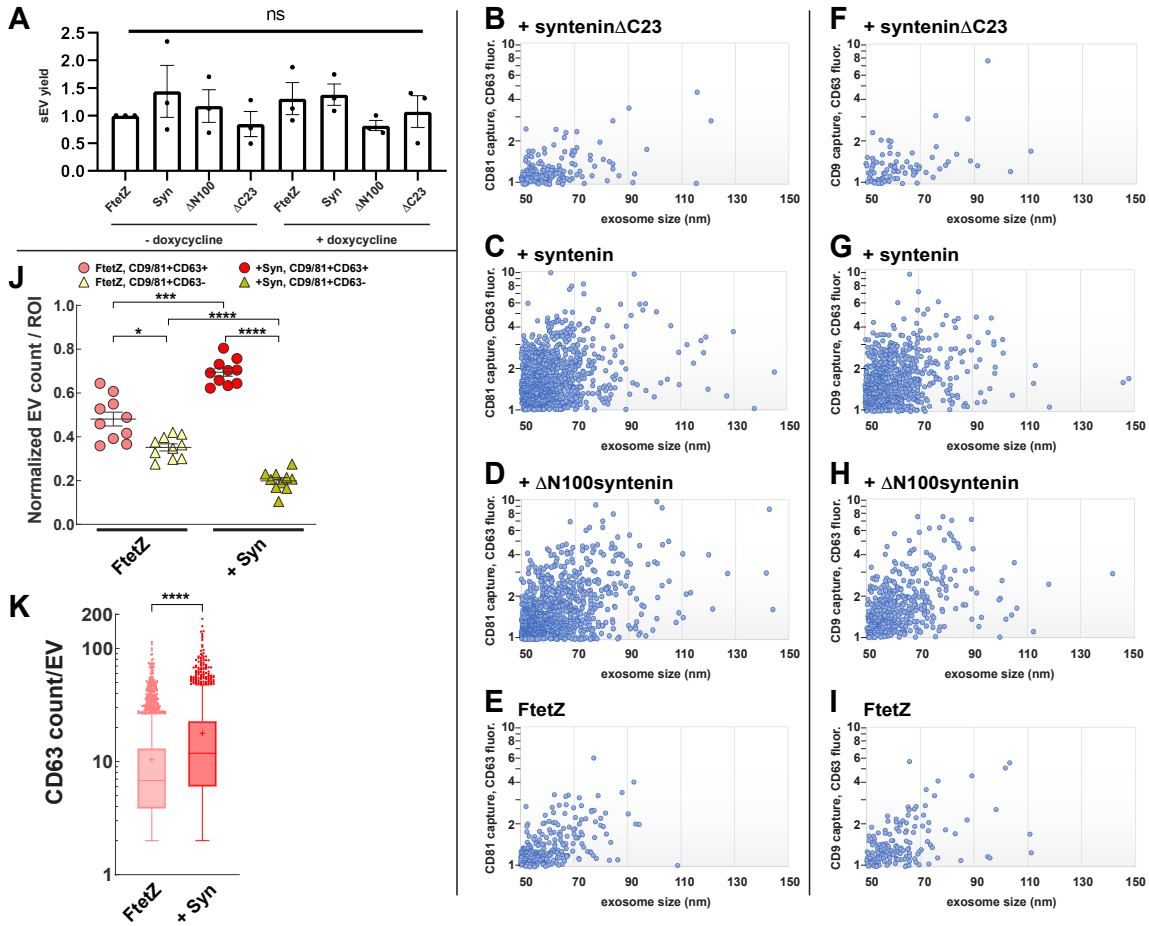

Figure 2. Syntenin drives the loading of CD63 into CD81 and CD9 exosomes. (**A**) Bar graph showing the yield of sEVs in exosome preparations collected from uninduced and induced FtetZ, FtetZ::syntenin. FtetZ::ΔN100syntenin, and FtetZ::synteninΔC23 cells. Bar height represents the average, error bars represent the standard error of the mean, and ANOVA showed that none of the differences approached the cutoff for statistical significance (p <0.05). (**B-E**) Scatter plot of (y-axis) anti-CD63 fluorescence (arbitrary units) of CD81-containing exosomes, plotted versus (x-axis) exosome size, as determined by SPIR-IFM imaging of exosomes produced by (B) FtetZ::synteninΔC23 cells, (C) FtetZ::syntenin cells, (D) FtetZ::ΔN100syntenin, and (E) FtetZ cells. (**F-I**) Scatter plot of (y-axis) anti-CD63 fluorescence (arbitrary units) of CD9-containing exosomes, plotted versus (x-axis) exosome size, as determined by SPIR-IFM imaging of exosomes produced by (F) FtetZ::synteninΔC23 cells, (G) FtetZ::syntenin cells, (H) FtetZ::ΔN100syntenin, and (I) FtetZ cells. (**J, K**) qSMLM-determined exosome immunophenotypes of CD81/CD9-immunopurified exosomes collected from doxycycline-induced FtetZ and FTetZ::syntenin cells, stained with AF647-labeled anti-CD63 and CF568-labeled anti-CD81 and anti-CD9 antibodies. (J) Scatter dot plot displaying the proportion of CD81/CD9-positive exosomes produced by FtetZ and FtetZ::syntenin cells that were (red dots) CD63 positive or (gold triangles) CD63 negative. Data are from 10 independent regions of interest (ROI) for each sample from two coverslips. Wide bars denote the average, and error bars denote the s.e.m. ****, ***, and * denote p values of <0.00005, <0.0005, and <0.05 from Dunnett's T3 multiple comparisons test. (K) Box and whisker plot showing the number of detected CD63 molecules per CD81/CD9-positive exosomes that had been produced by (left) FtetZ cells and (right) FtetZ::syntenin cells. **** denotes p value of <0.000001 from an unpaired t test with Welch's correction. Data is from two independent trials.

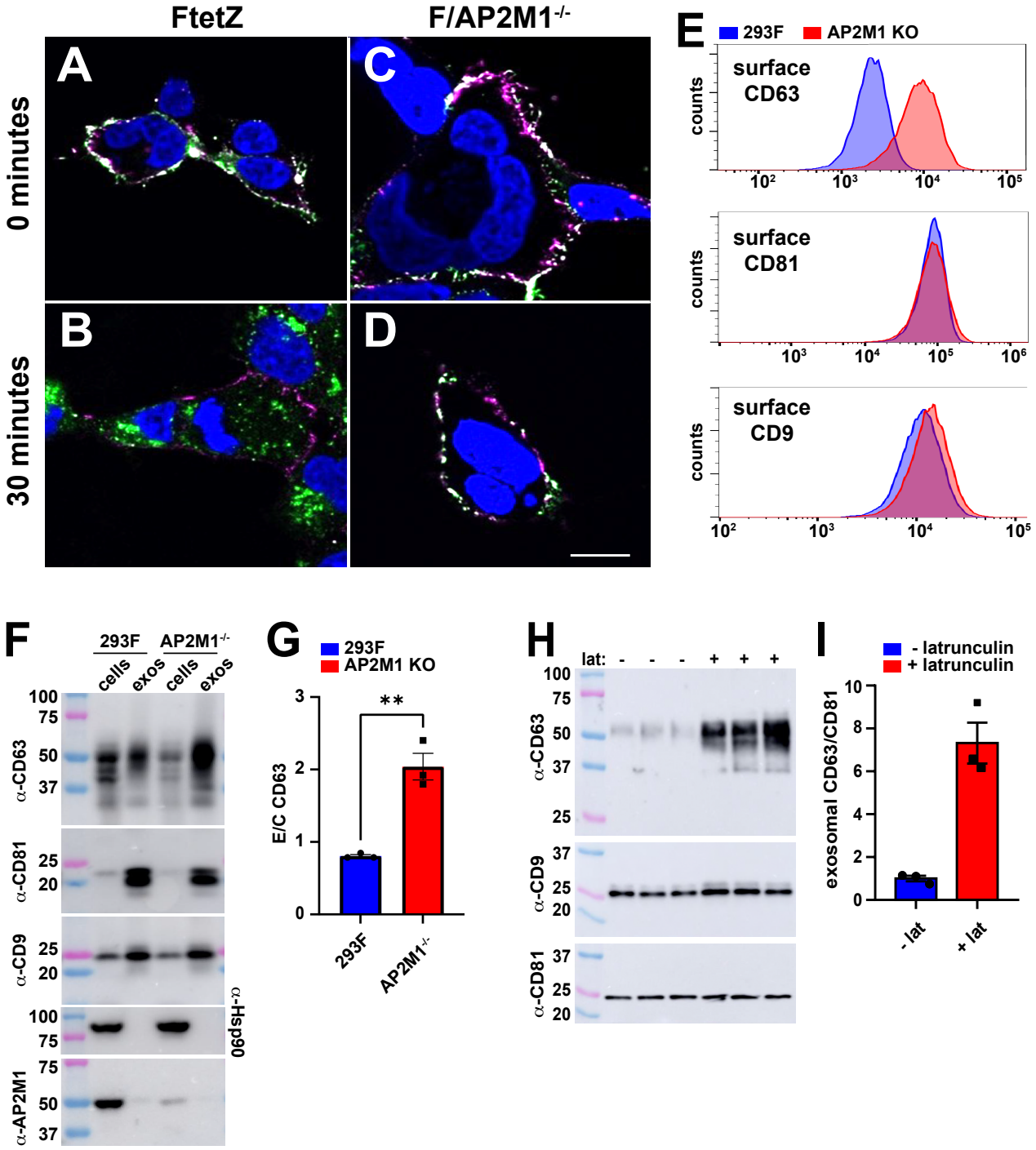

Figure 3. Inhibitors of endocytosis induce the exosomal secretion of CD63. (**A-D**) Confocal fluorescence micrographs of (A, B) 293F cells and (C, D) 293F/AP2M1$^{-/-}$ cells that had been chilled, incubated with fluorescent antibodies specific for (green) CD63 and (pink) CD9, washed, warmed to 37ºC, and then fixed after (A, C) 0 minutes at 37ºC or (B, D) 30 minutes at 37ºC. Bar, 10 um. (**E**) Histograms of flow cytometry data collected from 293F and 293F/AP2M1$^{-/-}$ cells that had been chilled and surface stained with fluorescently tagged antibodies specific for CD63, CD9, and CD81. (**F**) Immunoblot of cell and exosome fractions collected from 293F and AP2M1$^{-/-}$ cells, probed with antibodies specific for CD63, CD81, CD9, Hsp90, and AP2M1. (**G**) Bar graph showing the mean relative exosomal secretion of CD63 in 293F and 293F/AP2M1$^{-/-}$ cells, +/- s.e.m., calculated from immunoblot data. Student's t-test revealed a p value <0.005. (**H**) Immunoblot of

exosome fractions collected from 293F cells cultured in medium lacking or containing latrunculin A, probed with antibodies specific for CD63, CD9, and CD81. (**I**) Bar graph showing the mean CD63/CD81 ratio +/- s.e.m. in exosomes of 293F cells incubated in the absence or presence of latrunculin A. Student's t-test revealed a *p* value of 0.0028. All experiments were performed a minimum of three times. Dat is from three independent trials.

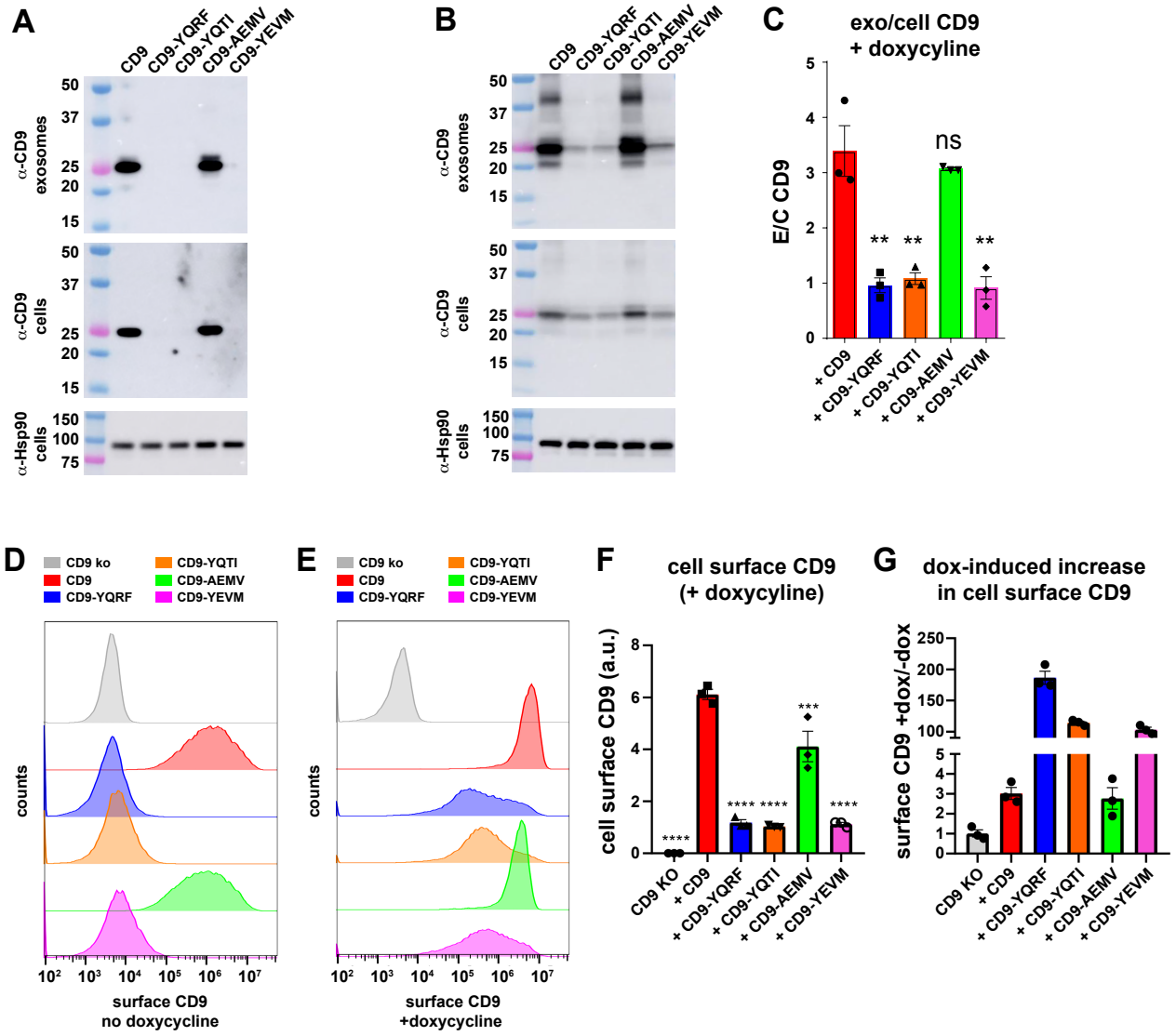

Figure 4. Endocytosis of CD9 inhibits its exosomal secretion and induces its lysosomal destruction. (**A, B**) Immunoblot of cell lysates and exosome lysates from (A) uninduced and (B) doxycycline-induced FtetZ/CD9$^{-/-/-}$ cells carrying TRE3G-regulated transgenes that express WT CD9, CD9-YQRF, CD9-YQTI, CD9-AEMV, or CD9-YEVM, probed with antibodies to CD9, with cell lysates also probed with antibodies to Hsp90. MW markers are in kDa. (**C**) Bar graphs showing the relative exosomal secretion of each CD9 protein from doxycycline-induced cell lines (amount of protein in exoxomes/amount of protein in cell). ** denotes an ANOVA p value of <0.005. (**D, E**) Histograms of anti-CD9 flow cytometry of (D) uninduced or (E) doxycycline-induced FtetZ/CD9$^{-/-/-}$ and FtetZ/CD9$^{-/-/-}$ cells carrying TRE3G-regulated transgenes that express WT CD9, CD9-YQRF, CD9-YQTI, CD9-AEMV, or CD9-YEVM. (**F**) Bar graph showing the mean +/- s.e.m. of cell surface CD9 staining, with **** and *** denoting ANOVA *p* values of <0.0005 and <0.005, respectively. (**G**) Bar graph showing the mean +/- s.e.m. of the fold difference in cell surface staining for CD9 in doxycycline-induced/uninduced cells. Data is from three independent trials.

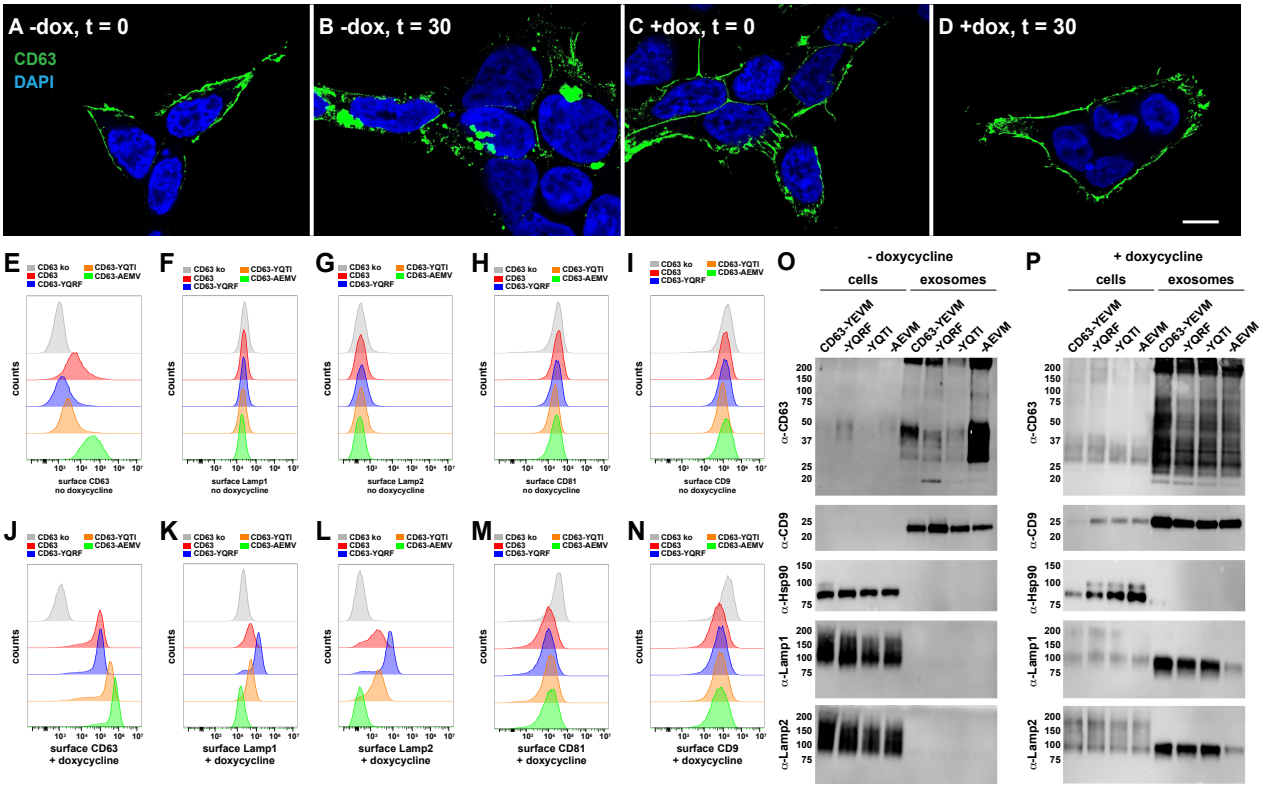

Figure 5. Endocytosis inhibits the exosomal secretion of CD63 while CD63 inhibits endocytosis. (**A-D**) Confocal fluorescence micrographs of FtetZ/CD63$^{-/-}$ ::CD63 cells grown in the (A, B) absence or (C, D) presence of doxycycline that had been chilled, incubated with a fluorescent antibody specific for (green) CD63, washed, fixed after (A, C) 0 minutes at 37ºC or (B, D) 30 minutes at 37ºC, then stained with DAPI. Bar, 10 um. (**E-I**) Histograms of flow cytometry data collected on uninduced (grey) FtetZ/CD63$^{-/-}$ cells and FtetZ/CD63$^{-/-}$ cells carrying TRE3G-regulated transgenes that express (red) WT CD63, (blue) CD63-YQRF, (orange) CD9-YQTI, or (green) CD63-AEMV, stained for cell surface (E) CD63, (F), Lamp1, (G) Lamp2, (H) CD81, or (I) CD9. (**J-N**) Histograms of flow cytometry data collected on doxycycline-induced (grey) FtetZ/CD63$^{-/-}$ cells and FtetZ/CD63$^{-/-}$ cells carrying TRE3G-regulated transgenes that express (red) WT CD63, (blue) CD63-YQRF, (orange) CD9-YQTI, or (green) CD63-AEMV, stained for cell surface (J) CD63, (K), Lamp1, (L) Lamp2, (M) CD81, or (N) CD9. (**O, P**) Immunoblot of cell and exosome lysates collected from (O) uninduced and (P) doxycycline-induced FtetZ/CD63$^{-/-}$ cells carrying TRE3G-regulated transgenes that express WT CD63, CD63-YQRF, CD9-YQTI, or CD63-AEMV. Blots were probed with antibodies specific for CD63, CD81, CD9, Lamp1, and Lamp2. MW size markers are listed in kDa. Data is from three independent trials.

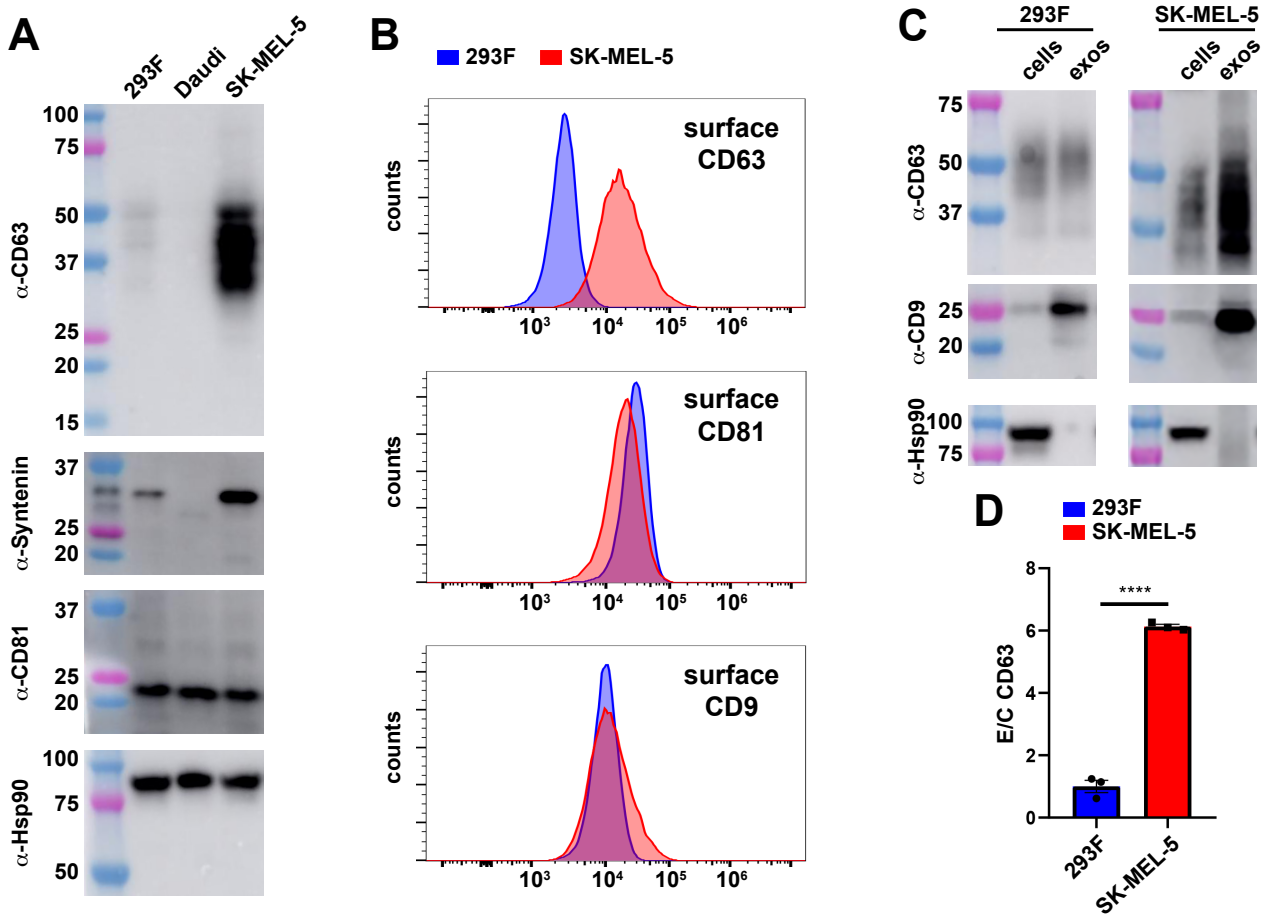

Figure 6. Natural elevation of CD63 expression also impairs endocytosis and induces its exosomal secretion. (**A**) Immunoblot of cell lysates collected from 293F, Daudi, and SK-MEL-5 cells using antibodies specific for CD63, syntenin, CD81, and Hsp90. MW size markers are listed in kDa. (**B**) Histograms of cell surface flow cytometry of 293F and SK-MEL-5 cells, stained with antibodies specific for CD63, CD81, and CD9. (**C**) Immunoblot of cell and exosomes lysates collected from 293F and SK-MEL-5 cells, probed with antibodies to CD63, CD9, and Hsp90. Bar graph showing the efficiency of CD63 budding (exosome/cell ratio) from 293F and SK-MEL-5 cells, with bar height representing the mean and error bars the s.e.m. (error bars). Data is from three independent trials.

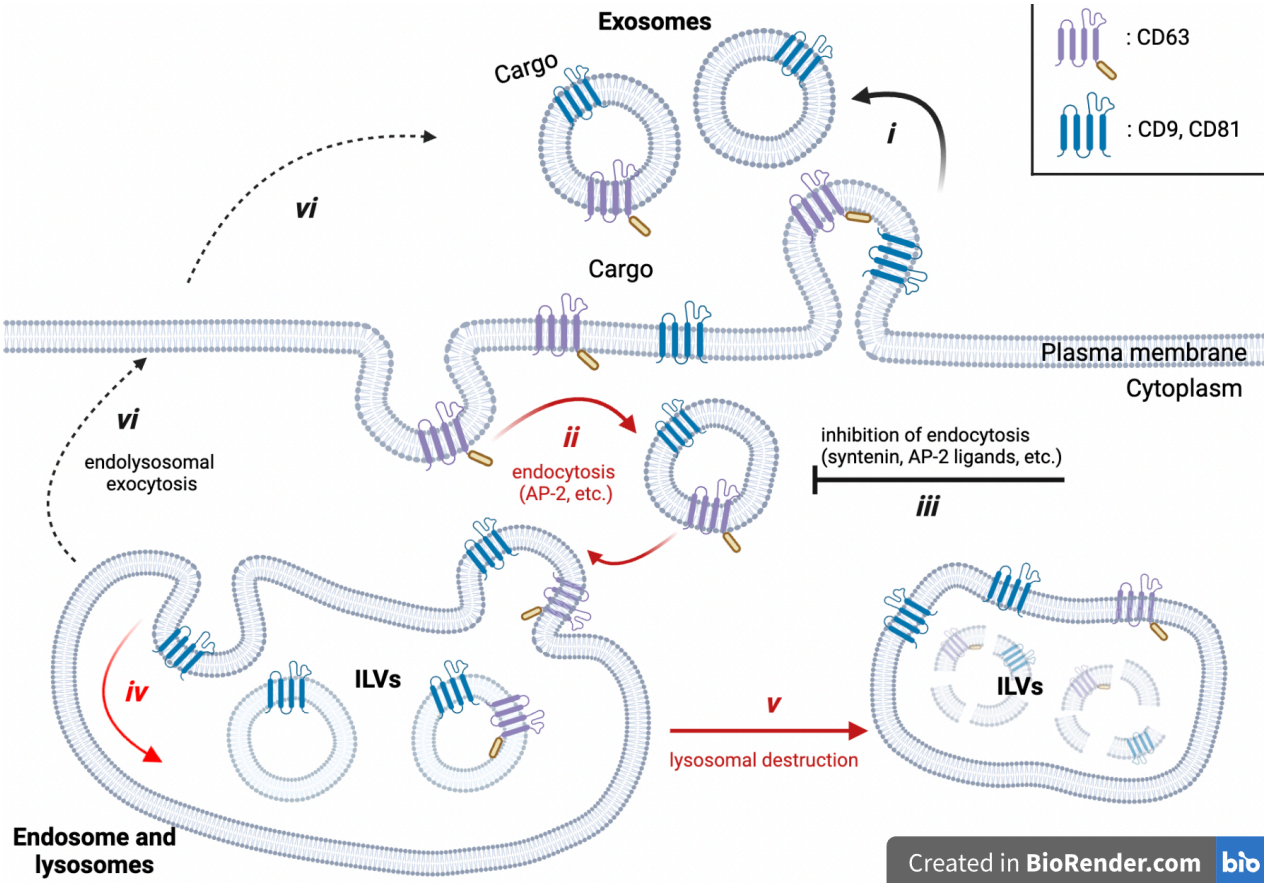

Figure 7. The shared, stochastic model of exosome biogenesis, updated. The plasma membrane is (***i***) the primary site of exosome biogenesis, and thus, the localization of exosome cargoes to the plasma membrane is the primary determinant of their exosomal secretion. Because the plasma membrane is the primary site of exosome biogenesis, the endocytosis of an exosome cargo protein will (***ii***) inhibit its exosomal secretion. Under this model, any factor that (***iii***) inhibits the endocytosis of an exosome cargo will (***i'***) induce its exosomal secretion from the cell, albeit indirectly, merely by increasing its steady-state abundance at the plasma membrane. This explains why the inhibition of CD63 endocytosis, whether by syntenin, mutation of AP2M1, inhibition of actin polymerization, or saturating inhibition of AP-2, induces the exosomal secretion of CD63, bringing its efficiency of exosomal secretion on par with plasma membrane-localized exosomes cargoes like CD81 and CD9. This model also explains the fate of endocytosed exosome cargo proteins, which are (***iv***) loaded into nascent ILVs that bud into the endosome lumen and then (***v***) delivered to lysosomes and degraded in lysosomes. This plasma membrane-to-lysosome degradative pathway can, however, be short-circuited by (***vi***) the exocytosis of ILV-containing endosomes and lysosomes, resulting the release of ILVs as exosomes, completing an endocytosis/exocytosis route of exosome biogenesis. Although this endocytosis/exocytosis pathway is slow, saturable, and secondary to the plasma membrane route of exosome biogenesis, it can mediate an *en bloc* release of stockpiled ILVs in response to specific signals.